Table 1 Patient characteristics

Arm	A (drainage alone)	B (ipc BLM)
N	42	38
Gender		
Male	27	24
Female	15	14
Median age (range)	60.5 (39–75)	60 (42–73)
Histology		
Small cell	3	2
Non-small cell	39	36
Prior chemotherapy		
Yes	29	24
No	13	14
Prior thoracic radiotherapy		
Yes	11	9
No	31	29
Drainage methods		
Surgical	19	17
Others	23	21
Median drainage volume in ml (range)	550 (250–1750)	600 (130–1930)
Effusion cytology		
Negative	6	11
Indeterminate	1	0
Positive	33	25
Not examined	2	2

ipc BLM = intrapericardial bleomycin instillation.

cytology-positive effusions in arm A. Cytology of the effusion was positive in 58 cases out of the 76 examined (76%).

In arm B, all 38 patients received at least one ipc BLM instillation and a total of 74 administrations: seven patients received four administrations (total BLM dose: 45 mg), five received three administrations (total BLM: 35 mg), five received two administrations (total BLM: 25 mg) and the remaining 21 received a single administration (total BLM: 15 mg). There was no apparent relationship between total dose and efficacy end points such as EFFS, except that those required four administrations had a worse primary control of the MPE.

A total of 24 patients (14 in arm A and 10 in arm B) received systemic chemotherapy after drainage tube removal. Nine patients (five in arm A and four in arm B) received gefitinib. Cytotoxic chemotherapy was administered to 21 patients (11 in arm A and 10 in arm B).

Morbidity and early deaths

Table 2 summarises the morbidity of the protocol therapy. Although 30 (38%) of the patients experienced some pain, no significant difference in the incidence and severity of pain was observed between the arms. Bleeding and infections were rare and generally controllable. Two patients in arm B developed transient fever of moderate degree (38–38.7°C). One case with constrictive pericarditis at 4 months and another with late cardiac dysfunction at 12 months after the registry, both reported to be grade 2, were observed in arm B.

As anticipated, there were as many as nine early deaths within 30 days of randomisation; five in arm A and four in arm B. Although the death was ascribed to disease progression in the majority, two patients in arm A died of massive bleeding during surgical attempts at re-drainage for recurrent MPE, possibly due to

Table 2 Morbidity of the protocol therapy

Arm	A (drainage alone)	B (ipc BLM)
N	42	38
Pain		
None	25	25
Medication not required	4	4
Controlled with non-opioid analgesics	9	7
Controlled with opioid analgesics	4	2
Uncontrollable	0	0
Infection		
None	39	35
Controllable	3	3
Uncontrollable	0	0
Bleeding		
None	42	36
Controllable	0	1
Severe	0	1
Late complications		
None	42	36
Pulmonary	0	0
Cardiac function	0	1 (grade 2)
Constrictive pericarditis	0	1 (grade 2)

ipc BLM = intrapericardial bleomycin instillation.

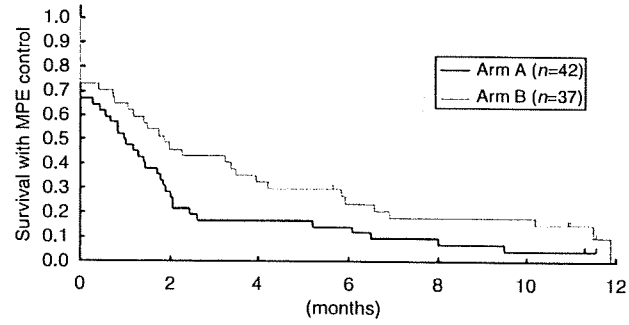

Figure 1 Effusion failure-free survival (EFFS). The median EFFS was 30 days in arm A and 57 days in arm B, with a hazard ratio of 0.64 (95% confidence interval: 0.40–1.03), with arm B significantly favouring this parameter (one-sided $P = 0.030$ by log-rank test).

crack formation in the ventricular wall upon dissection of the adherent pericardium. Another patient in arm B died suddenly on day 12 of the protocol without a clear cause.

Efficacy end points

Primary control of the MPE with successful tube removal within 7 days of randomisation was achieved in 28 of the 42 cases (67%) in arm A and 27 of the 37 eligible cases (73%) in arm B, the difference between the two groups not being statistically significant. The median time to tube removal was 7 days in each arm. Arm B favoured EFFS (Figure 1), with a hazard ratio of 0.64 (95% confidence interval: 0.40–1.03, and one-sided $P = 0.030$ by log-rank test).

The EFFS at 1, 2, 4, 6 and 12 months was 50, 29, 17, 14 and 5%, respectively, for arm A, and 65, 46, 32, 24 and 10%, respectively, for arm B. Although arm B also favoured the primary end point, EFFS at 2 months (46 *vs* 29%), the difference between the two

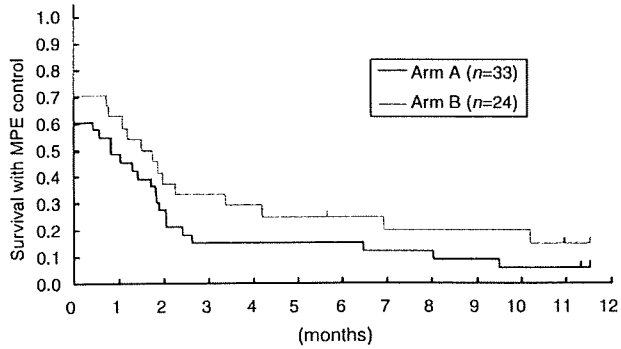

Figure 2 Effusion failure-free survival (EFFS) in effusion cytology-positive patients. In the effusion cytology-positive patient subset, arm B favoured EFFS. The hazard ratio was 0.69 (95% confidence interval: 0.39–1.21).

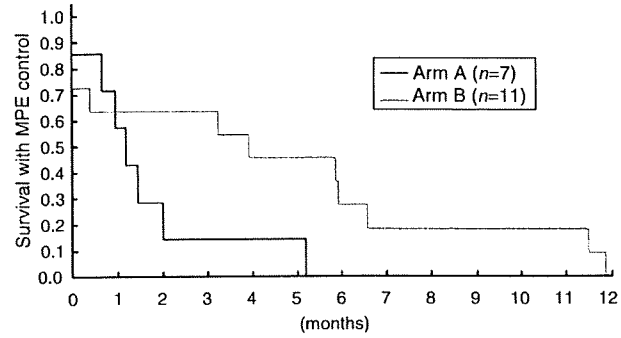

Figure 3 Effusion failure-free survival (EFFS) in effusion cytology-negative or -indeterminate patients. In the effusion cytology-negative or -indeterminate patient subset, arm B favoured EFFS. The hazard ratio was 0.39 (95% confidence interval: 0.12–1.21).

groups was not statistically significant (one-sided $P = 0.086$ by Fisher's exact test).

The median OS was not significantly different between the two arms: 79 days in arm A and 119 days in arm B. The OS rates at 6 months were 27 and 31% in arm A and arm B, respectively.

Subgroup analysis

As more patients in arm A had cytology-positive effusion, which has been reported to be associated with a poor prognosis (Gornik *et al*, 2005), subset analysis was performed according to the effusion cytology status (Figures 2 and 3). In both cytology-positive patients (Figure 2) and cytology-negative or -indeterminate patients (Figure 3), arm B favoured EFFS.

Thirty-six patients had undergone surgical (subxiphoid pericardiostomy) and 43 had undergone non-surgical (percutaneous tube pericardiostomy) drainage before randomisation. Patients with surgical drainage tended to have a longer EFFS (Figure 4). The effect of ipc BLM was observed irrespective of the drainage method employed; arm B tended to favour EFFS both in patients with surgical drainage (hazard ratio 0.62, 95% confidence interval: 0.30–1.29) and in those with non-surgical drainage (hazard ratio 0.56, 95% confidence interval: 0.29–1.05).

Symptom palliation

The baseline symptom scores were taken for all of the 79 eligible patients, at enrolment (after drainage). At the 1-month follow-up,

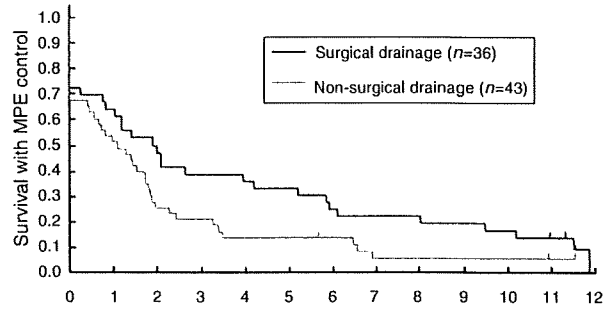

Figure 4 Effusion failure-free survival (EFFS) and drainage method. Patients with surgical drainage tended to have longer EFFS (median EFFS: 2.0 *vs* 1.1 month).

Table 3 Symptom palliation

Arm	A (drainage alone)	B (ipc BLM)
N eligible	42	37
% of those with improved or stable scores[a]		
Cough	60%	57%
Pain	50%	62%
Anorexia	55%	62%
Dyspnoea	62%	46%
Total	55%	51%

ipc BLM = intrapericardial bleomycin instillation. [a]The scores at 1 month were compared with those at enrolment.

approximately half of the patients (55% in arm A and 51% in arm B) had stable or improved overall scores. There were no significant differences between the arms for any of the symptom scores (Table 3).

DISCUSSION

Malignant pericardial effusion is a potentially life-threatening complication of malignancy that usually manifests itself at an advanced or terminal stage of the disease. It brings great agony to the patient once it becomes symptomatic, with dyspnoea, orthopnoea, chest pain and cough. Although the prognosis of the patients with MPE is very poor, especially in those with chemotherapy-resistant tumours such as non-small-cell lung cancer (Press and Livingston, 1987; Okamoto *et al*, 1993; Gornik *et al*, 2005; Yonemori *et al*, 2007), optimal management is very important for palliation.

Pericardial sclerosis following drainage has been widely performed. However, data are available mainly from phase II trials or case series. In fact, historical comparison has failed to demonstrate the efficacy of pericardial sclerosis over drainage alone (Okamoto *et al*, 1993; Vaitkus *et al*, 1994). It has also been suggested that sclerosis may be effective in preventing re-accumulation of MPE after percutaneous tube pericardiostomy, but not after subxiphoid pericardiotomy, because the surgical intervention alone was considered to be sufficient to prevent recurrent MPE (Press and Livingston, 1987; Park *et al*, 1991; McDonald *et al*, 2003).

In addition, there are some potential morbidities associated with pericardial sclerosis; most of the agents used as sclerosants produce unpleasant adverse effects, such as fever and pain (Liu *et al*, 1996). There is also concern about the complications of the procedure, both in the short term, such as bleeding and infection,

and in the long term, such as constrictive pericarditis, as the inflammatory response causes adhesion of the visceral and parietal pericardium (Shepherd, 1997).

We undertook a randomised trial to evaluate the efficacy of pericardial sclerosis following drainage as compared with drainage alone. We chose BLM as the sclerosant agent for ipc instillation, because of its low toxicity as compared with doxycycline, reported from an earlier randomised trial (Liu *et al*, 1996). We included only patients with non-small-cell lung cancer or chemotherapy-treated small cell cancer to minimise the influence of systemic chemotherapy after the protocol study (Vaitkus *et al*, 1994). We randomised the patients after the pericardial drainage, as we judged that obtaining informed consent before it, that is when the patients suffer from symptoms of MPE, would be very difficult. Therefore, we did not specify the indication for drainage and enrolled cases after both emergent and elective drainage. We thus focused on the prevention of MPE recurrence. We could not find any comparable phase III trial on this participant, and no such trial is registered in ClinicalTrial gov.

We found that ipc BLM instillation seemed to be effective at preventing the recurrence of MPE. However, the benefit in the primary end point, that is, EFFS at 2 months, was not significantly different, which is a major drawback to make a definitive conclusion. The therapeutic benefit, which could not be demonstrated with our modestly sample-sized trial, therefore, might be only a modest one. On the other hand, the benefit of ipc BLM seemed to be unrelated to the drainage method. As expected, the OS was poor in both arms and not significantly different.

Our study has several limitations. One is that without significant survival prolongation and difference of symptom scores, modest improvement of the EFFS might not represent true patient benefit. We believe, however, that conductance of our trial itself would be fully justified; given the severe symptoms of uncontrolled MPE and the inconvenience of the drainage tube, survival without MPE would be a worthwhile treatment goal.

The second limitation was that we limited the participants to lung cancer patients, which makes it difficult to evaluate late complications due to short OS. In patients with more chemotherapy-sensitive tumours such as breast cancer or lymphoma, many more patients may be expected to live for up to at least 1 year longer. There would be greater concern about late pericardial or cardiac complications, which we did observe in two of our own cases. Even for lung cancer patients, advances in systemic therapy may be expected to improve the outcome of those with even far-advanced disease in the future, which would evidently modify the risk/benefit of ipc BLM.

The third limitation of our study was that we did not control for the method of primary pericardial drainage, and each institution chose it in accordance with its daily practice. We do not believe that our results were much biased by the drainage methods, as each participating institution basically adhered to one method of its choice, and the ipc BLM arm tended to favour EFFS in both subgroups with surgical and non-surgical drainage. However, control for the drainage method or indication (emergent *vs* elective) for drainage might be necessary in future trials, as they might well affect the patient outcomes. In fact, we did observe that, although not a randomised comparison and thus it should be interpreted with caution, patients who underwent surgical drainage tended to have a better MPE control.

Recently, less invasive techniques for surgical treatment of MPE have been described, such as percutaneous balloon pericardiotomy (Ziskind *et al*, 1993; Wang *et al*, 2002), which create a pleuro-pericardial communication and allow fluid drainage into pleural space. It was reported to be effective and safe, and may potentially obviate the need for surgical intervention. However, it has yet to be compared with other drainage methods and its role has not been established. No patient underwent this procedure in our study.

One ancillary finding of our study was that two patients died of major bleeding during surgical attempts at re-drainage for recurrent MPE. Although it has rarely been reported in the literature, partial adhesions could have led to injury to the cardiac wall during the surgical procedure.

In this trial, we evaluated the safety and efficacy of pericardial sclerosis with a 'classic' sclerosant agent of BLM. Future trial designs would include one to compare BLM with another agent with a different mode of action, such as intrapericardial instillation of a platinum compound as 'local chemotherapy'.

In conclusion, we found that pericardial sclerosis with ipc BLM after drainage appears to be safe and effective, overall, in the management of MPE in patients with lung cancer and should be a valid therapeutic option in these patients. We could not, however, demonstrate a statistical significance in the primary end point with the modest sample size of 80. The therapeutic advantage might not be large enough, and more trials are warranted.

ACKNOWLEDGEMENTS

We thank the members of the JCOG data center and operations office for their support in preparing the paper and oversight of the study management (Drs Isamu Saito and Haruhiko Fukuda), statistical analysis (Mr Takashi Asakawa and Dr Naoki Ishizuka) and data management (Mr Hidenobu Yamada).

Conflict of interest

The authors have no conflicts of interest to declare.
Registered in www.clinicaltrials.gov, ClinicalTrials.gov number, NCT00132613 and in UMIN-CTR[www.umin.ac.jp/ctr/], identification number, C000000030.

REFERENCES

Abraham KP, Reddy V, Gattuso P (1990) Neoplasms metastatic to the heart: review of 3314 consecutive autopsies. *Am J Cardiovasc Pathol* **3**: 195–198

Colleoni M, Martinelli G, Beretta F, Marone C, Gallino A, Fontana M, Graffeo R, Zampino G, De Pas T, Cipolla G, Martinoni C, Goldhirsch A (1998) Intracavitary chemotherapy with thiotepa in malignant pericardial effusions: an active and well-tolerated regimen. *J Clin Oncol* **16**: 2371–2376

Dempke W, Firusian N (1999) Treatment of malignant pericardial effusion with 32P-colloid. *Br J Cancer* **80**: 1955–1957

Gornik HL, Gerhard-Herman M, Beckman JA (2005) Abnormal cytology predicts poor prognosis in cancer patients with pericardial effusion. *J Clin Oncol* **23**: 5211–5216

Imamura T, Tamura K, Takenaga M, Nagatomo Y, Ishikawa T, Nakagawa S (1991) Intrapericardial OK-432 instillation for the management of malignant pericardial effusion. *Cancer* **68**: 259–263

Kaira K, Takise A, Kobayashi G, Utsugi M, Horie T, Mori T, Imai H, Inazawa M, Mori M (2005) Management of malignant pericardial effusion with instillation of mitomycin C in non-small cell lung cancer. *Jpn J Clin Oncol* **35**: 57–60

Kawashima O, Kurihara T, Kamiyoshihara M, Sakata S, Ishikawa S, Morishita Y (1999) Management of malignant pericardial effusion resulting from recurrent cancer with local instillation of aclarubicin hydrochloride. *Am J Clin Oncol* **22**: 396–398

Klatt EC, Heitz DR (1990) Cardiac metastases. *Cancer* **65**: 1456–1459

Lerner-Tung MB, Chang AY, Ong LS, Kreiser D (1997) Pharmacokinetics of intrapericardial administration of 5-fluorouracil. *Cancer Chemother Pharmacol* **40**: 318–320

Liu G, Crump M, Goss PE, Dancey J, Shepherd FA (1996) Prospective comparison of the sclerosing agents doxycycline and bleomycin for the primary management of malignant pericardial effusion and cardiac tamponade. *J Clin Oncol* **14**: 3141–3147

Maher EA, Shepherd FA, Todd TJ (1996) Pericardial sclerosis as the primary management of malignant pericardial effusion and cardiac tamponade. *J Thorac Cardiovasc Surg* **112**: 637–643

Martinoni A, Cipolla CM, Cardinale D, Civelli M, Lamantia G, Colleoni M, Fiorentini C (2004) Long-term results of intrapericardial chemotherapeutic treatment of malignant pericardial effusions with thiotepa. *Chest* **126**: 1412–1416

Maruyama R, Yokoyama H, Seto T, Nagashima S, Kashiwabara K, Araki J, Semba H, Ichinose Y (2007) Catheter drainage followed by the instillation of bleomycin to manage malignant pericardial effusion in non-small cell lung cancer: a multi-institutional phase II trial. *J Thorac Oncol* **2**: 65–68

McDonald JM, Meyers BF, Guthrie TJ, Battafarano RJ, Cooper JD, Patterson GA (2003) Comparison of open subxiphoid pericardial drainage with percutaneous catheter drainage for symptomatic pericardial effusion. *Ann Thorac Surg* **76**: 811–815; discussion 816

Moriya T, Takiguchi Y, Tabeta H, Watanabe R, Kimura H, Nagao K, Kuriyama T (2000) Controlling malignant pericardial effusion by intrapericardial carboplatin administration in patients with primary non-small-cell lung cancer. *Br J Cancer* **83**: 858–862

Norum J, Lunde P, Aasebo U, Himmelmann A (1998) Mitoxantrone in malignant pericardial effusion. *J Chemother* **10**: 399–404

Okamoto H, Shinkai T, Yamakido M, Saijo N (1993) Cardiac tamponade caused by primary lung cancer and the management of pericardial effusion. *Cancer* **71**: 93–98

Park JS, Rentschler R, Wilbur D (1991) Surgical management of pericardial effusion in patients with malignancies. Comparison of subxiphoid window *vs* pericardiectomy. *Cancer* **67**: 76–80

Press OW, Livingston R (1987) Management of malignant pericardial effusion and tamponade. *JAMA* **257**: 1088–1092

Primrose WR, Clee MD, Johnston RN (1983) Malignant pericardial effusion managed with Vinblastine. *Clin Oncol* **9**: 67–70

Shepherd FA (1997) Malignant pericardial effusion. *Curr Opin Oncol* **9**: 170–174

Shepherd FA, Morgan C, Evans WK, Ginsberg JF, Watt D, Murphy K (1987) Medical management of malignant pericardial effusion by tetracycline sclerosis. *Am J Cardiol* **60**: 1161–1166

Theologides A (1978) Neoplastic cardiac tamponade. *Semin Oncol* **5**: 181–192

Tobinai K, Kohno A, Shimada Y, Watanabe T, Tamura T, Takeyama K, Narabayashi M, Fukutomi T, Kondo H, Shimoyama M, Suemasu K (1993) Toxicity grading criteria of the Japan Clinical Oncology Group. The Clinical Trial Review Committee of the Japan Clinical Oncology Group. *Jpn J Clin Oncol* **23**: 250–257

Tomkowski WZ, Wisniewska J, Szturmowicz M, Kuca P, Burakowski J, Kober J, Fijalkowska A (2004) Evaluation of intrapericardial cisplatin administration in cases with recurrent malignant pericardial effusion and cardiac tamponade. *Support Care Cancer* **12**: 53–57

Vaitkus PT, Herrmann HC, LeWinter MM (1994) Treatment of malignant pericardial effusion. *JAMA* **272**: 59–64

Wang HJ, Hsu KL, Chiang FT, Tseng CD, Tseng YZ, Liau CS (2002) Technical and prognostic outcomes of double-balloon pericardiotomy for large malignancy-related pericardial effusions. *Chest* **122**: 893–899

Wilkes JD, Fidias P, Vaickus L, Perez RP (1995) Malignancy-related pericardial effusion. 127 cases from the Roswell Park Cancer Institute. *Cancer* **76**: 1377–1387

Yonemori K, Kunitoh H, Tsuta K, Tamura T, Arai Y, Shimada Y, Fujiwara Y, Sasajima Y, Asamura H, Tamura T (2007) Prognostic factors for malignant pericardial effusion treated by pericardial drainage in solid-malignancy patients. *Med Oncol* **24**: 425–430

Ziskind AA, Pearce AC, Lemmon CC, Burstein S, Gimple LW, Herrmann HC, McKay R, Block PC, Waldman H, Palacios IF (1993) Percutaneous balloon pericardiotomy for the treatment of cardiac tamponade and large pericardial effusions: description of technique and report of the first 50 cases. *J Am Coll Cardiol* **21**: 1–5

Appendix

Supported by the Grant-in-Aid for Cancer Research from the Ministry of Health, Labour and Welfare of Japan (11S-2, 11S-4, 14S-2, 14S-4, 17S-2, 17S-5).

Presented in part at the 43rd Annual Meeting of the American Society of Clinical Oncology, June 1–5, 2007, Chicago IL.

Study participants: The following institutions and investigators participated in the trial:

National Hospital Organization Dohoku Hospital (Yuka Fujita and Satoru Fujiuchi), Tochigi Cancer Center (Kiyoshi Mori and Yukari Kamiyama), National Cancer Center Hospital East (Kaoru Kubota, Yutaka Nishiwaki and Nagahiro Saijo), National Cancer Center Hospital (Noboru Yamamoto, Tomohide Tamura and Hideo Kunitoh), International Medical Center (Koichiro Kudo and Yuichiro Takeda), Cancer Institute Hospital (Takeshi Horai and Makoto Nishio), Kanagawa Cancer Center (Kazumasa Noda and Fumihiro Oshita), Yokohama Municipal Citizen's Hospital (Koshiro Watanabe and Hiroaki Okamoto), Niigata Cancer Center Hospital (Akira Yokoyama and Yuko Tsukada), Gifu City Hospital (Yoshiyuki Sawa and Takashi Ishiguro), Aichi Cancer Center Hospital (Toyoaki Hida), National Hospital Organization Nagoya Medical Center (Hideo Saka), Kinki University Hospital (Kazuhiko Nakagawa and Isamu Okamoto) and Kyushu University Hospital (Yoichi Nakanishi and Koichi Takayama).

VOLUME 27 · NUMBER 13 · MAY 1 2009

JOURNAL OF CLINICAL ONCOLOGY ORIGINAL REPORT

Identification of a Predictive Biomarker for Hematologic Toxicities of Gemcitabine

Junichi Matsubara, Masaya Ono, Ayako Negishi, Hideki Ueno, Takuji Okusaka, Junji Furuse, Koh Furuta, Emiko Sugiyama, Yoshiro Saito, Nahoko Kaniwa, Junichi Sawada, Kazufumi Honda, Tomohiro Sakuma, Tsutomu Chiba, Nagahiro Saijo, Setsuo Hirohashi, and Tesshi Yamada

From the Chemotherapy Division, National Cancer Center Research Institute; Hepatobiliary and Pancreatic Oncology Division and Clinical Laboratory Division, National Cancer Center Hospital; Project Team for Pharmacogenetics, National Institute of Health Sciences; BioBusiness Group, Mitsui Knowledge Industry, Tokyo; Hepatobiliary and Pancreatic Oncology Division, National Cancer Center Hospital East, Kashiwa; and Department of Gastroenterology and Hepatology, Kyoto University Graduate School of Medicine, Kyoto, Japan.

Submitted September 3, 2008; accepted December 1, 2008; published online ahead of print at www.jco.org on March 16, 2009.

Supported by the Program for Promotion of Fundamental Studies in Health Sciences conducted by the National Institute of Biomedical Innovation of Japan, the Third-Term Comprehensive Control Research for Cancer conducted by the Ministry of Health and Labor of Japan, and generous grants from the Naito Foundation, the Princess Takamatsu Cancer Research Fund, and the Foundation for the Promotion of Cancer Research. These sponsors had no role in the design of the study, the collection of the data, the analysis and interpretation of the data, the decision to submit the article for publication, or the writing of the article.

Authors' disclosures of potential conflicts of interest and author contributions are found at the end of this article.

Corresponding author: Tesshi Yamada, MD, PhD, Chemotherapy Division, National Cancer Center Research Institute, 5-1-1 Tsukiji, Chuo-ku, Tokyo 104-0045, Japan; e-mail: tyamada@ncc.go.jp.

The Appendix is included in the full-text version of this article, available online at www.jco.org. It is not included in the PDF version (via Adobe® Reader®).

0732-183X/09/2713-2261/$20.00

DOI: 10.1200/JCO.2008.19.9745

ABSTRACT

Purpose
Gemcitabine monotherapy is the current standard for patients with advanced pancreatic cancer, but the occurrence of severe neutropenia and thrombocytopenia can sometimes be life threatening. This study aimed to discover a new diagnostic method for predicting the hematologic toxicities of gemcitabine.

Patients and Methods
Using quantitative mass spectrometry (MS), we compared the baseline plasma proteomes of 25 patients who had developed severe hematologic adverse events (grade 3 to 4 neutropenia and/or grade 2 to 4 thrombocytopenia) within the first two cycles of gemcitabine with those of 22 patients who had not (grade 0).

Results
We identified 757 peptide peaks whose intensities were significantly different ($P < .001$, Welch t test) among a total of 60,888. The MS peak with the highest statistical significance ($P = .0000282$) was revealed to be derived from haptoglobin by tandem MS. A scoring system (nomogram) based on the values of haptoglobin, haptoglobin phenotype, neutrophil count, platelet count, and body-surface area was constructed to estimate the risk of hematologic adverse events (grade 3 to 4 neutropenia and/or grade 2 to 4 thrombocytopenia) with an area under curve value of 0.782 in a cohort of 166 patients with pancreatic cancer. Predictive ability of the system was confirmed in two independent validation cohorts consisting of 87 and 52 patients with area under the curve values of 0.655 and 0.747, respectively.

Conclusion
Although the precise mechanism responsible for the correlation of haptoglobin with the future onset of hematologic toxicities remains to be clarified, our prediction model seems to have high practical utility for tailoring the treatment of patients receiving gemcitabine.

J Clin Oncol 27:2261-2268. © 2009 by American Society of Clinical Oncology

INTRODUCTION

Pancreatic adenocarcinoma is one of the most aggressive and lethal cancers.[1] It is the fifth leading cause of cancer-related mortality in Japan and the fourth leading cause in the United States, accounting for an estimated more than 23,000 annual deaths in Japan and more than 33,000 deaths in the United States.[2,3] The median survival time of patients with advanced pancreatic cancer had remained at only 3 to 4 months until the introduction of the nucleoside anticancer drug gemcitabine (2′,2′-difluorodeoxycytidine). Gemcitabine monotherapy extended the overall survival of pancreatic cancer patients up to 6 months, along with significant clinical benefits such as pain relief and improvement of performance status,[4-6] and is now accepted as a standard first-line treatment for unresectable advanced pancreatic cancer.[7] However, hematologic toxicity is the dose-limiting factor of gemcitabine therapy.[8] Although severe nonhematologic toxicity is infrequent,[4-6] 20% to 30% of patients receiving gemcitabine experience grade 3 to 4 neutropenia (National Cancer Institute [NCI] Common Toxicity Criteria, version 2.0), and approximately 10% experience grade 3 to 4 thrombocytopenia.[5,6,9,10] These levels of severe hematologic adverse events (AEs) can be potentially life threatening.

Several attempts have been made to predict the occurrence of AE associated with chemotherapy. Old age, poor performance status, and reduced initial blood cell counts have been reported to be the risk factors of hematotoxicities.[11,12] To further improve prediction accuracy, combinations of these

risk factors have also been proposed,[11-14] but no reliable predictor has been established for gemcitabine-induced hematologic AEs. We previously identified a significant correlation of a nonsynonymous single nucleotide polymorphism of the cytidine deaminase (*CDA*) gene with altered pharmacokinetics of gemcitabine, but its prediction accuracy for hematologic AE was not satisfactory.[15,16]

Recent advanced proteomic technologies have been increasingly applied to studies of clinical samples[17] to identify biomarkers that could facilitate the tailoring of cancer treatments. Protein expression is not always correlated with mRNA expression,[18] and it is anticipated that alterations in the protein content of clinical samples more directly reflect the biologic and pathologic status of patients. Matrix-assisted laser desorption/ionization mass spectrometry (MS) is becoming a method of choice for profiling of clinical samples as a result of its high sensitivity and throughput. In fact, previous studies have successfully identified biomarkers that could predict the outcome of cancer patients and the efficacy of molecular-targeting drugs.[19,20] However, only low molecular weight proteins can be analyzed by matrix-assisted laser desorption/ionization MS, and thus, a method allowing more comprehensive protein profiling is desirable.

Shotgun proteomics is an emerging concept in which whole proteins are enzymatically digested into a large array of small peptide fragments having uniform physical and chemical characteristics and then analyzed directly by MS. We previously developed a new platform, namely two-dimensional image converted analysis of liquid chromatography and mass spectrometry (2DICAL), to give a quantitative dimension to shotgun proteomics.[21] To identify new biomarkers that might be useful for prediction of gemcitabine-induced neutropenia and thrombocytopenia in patients with pancreatic cancer, we compared the plasma protein profiles of two extreme populations of patients who had shown different responses to the same gemcitabine treatment by 2DICAL. Here we report the identification of plasma/serum haptoglobin as a biomarker of hematologic toxicities associated with gemcitabine treatment.

PATIENTS AND METHODS

Patients

Plasma or serum samples were collected from three cohorts (modeling [M0], validation-1 [V1], and validation-2 [V2] cohorts) totaling 305 patients. All the patients had locally advanced or metastatic (stage IVA or IVB),[22] histologically or cytologically proven pancreatic ductal adenocarcinoma and received at least two cycles of gemcitabine monotherapy (1,000 mg/m^2 intravenously over 30 minutes on days 1, 8, and 15 of a 28-day cycle). Demographic and laboratory data for the patients before administration of gemcitabine are listed in Appendix Tables A1 to A3 (online only). The severity of early hematologic AEs that appeared within the first two cycles of the gemcitabine treatment was graded according to NCI Common Terminology Criteria for Adverse Events (CTCAE; version 3.0).

Cohort M0 comprised 166 patients who had been enrolled onto our previous study at the National Cancer Center (NCC) Hospital (Tokyo, Japan) and Hospital East (Kashiwa, Japan) between September 2002 and July 2004.[15,16] Cohort V1 comprised 87 patients who had been treated consecutively at the NCC Hospital between August 2005 and June 2007, and cohort V2 comprised 52 patients treated at the NCC Hospital consecutively between August 2004 and July 2005.

Sample Preparation

Blood was drawn before the administration of gemcitabine. Plasma (cohorts M0 and V1) or serum (cohort V2) was separated by centrifugation at 4°C and frozen at −70°C (cohort M0) or −20°C (cohorts V1 and V2) until analysis. Macroscopically hemolyzed samples were excluded from the current analysis. The protocol of this retrospective study was reviewed and approved by the institutional ethics committee boards of the NCC (Tokyo, Japan) and the National Institute of Health Sciences (Tokyo, Japan).

Liquid Chromatography/MS

Samples were passed through an IgY-12 High Capacity Spin Column (Beckman Coulter, Fullerton, CA) in accordance with the manufacturer's instructions to reduce the amounts of the 12 most abundant plasma proteins. The flow-through portion was digested with sequencing-grade modified trypsin (Promega, Madison, WI) and analyzed in triplicate using a nano-flow high-performance liquid chromatograph (NanoFrontier nLC; Hitachi High-Technologies, Tokyo, Japan) connected to an electrospray ionization quadrupole time-of-flight (ESI-Q-TOF) mass spectrometer (Q-Tof Ultima; Waters, Milford, MC).

MS peaks were detected, normalized, and quantified using the in-house 2DICAL software package, as described previously.[21] A serial identification (ID) number was applied to each of the MS peaks detected (1 to 60,888). The stability of liquid chromatography/MS was monitored by calculating the correlation coefficient of every triplicate measurement. The mean correlation coefficient (±standard deviation) of the entire 60,888 peaks of the 47 triplicate runs was as high as 0.978 (±0.017).

Tandem MS

Peak lists were generated using the Mass Navigator software package (version 1.2; Mitsui Knowledge Industry, Tokyo, Japan) and searched against the SwissProt database (downloaded from http://www.expasy.ch/sprot/sprot-top.html on October 18, 2007) using the Mascot software package (version 2.2.1; Matrix Science, London, United Kingdom). The score threshold was set to $P < .05$ based on the size of the database used in the search.

Western Blot Analysis

Primary antibodies used were rabbit polyclonal antibody against human haptoglobin (Dako, Glostrup, Denmark) and mouse monoclonal antibody against human complement C3b-α (Progen, Heidelberg, Germany). Ten microliters of partitioned sample were separated by sodium dodecyl sulfate–polyacrylamide gel electrophoresis (SDS-PAGE) and electroblotted onto a polyvinylidene difluoride membrane. The membrane was then incubated with the primary antibody and subsequently with relevant horseradish peroxidase–conjugated antirabbit or antimouse immunoglobulin G as described previously.[23,24] Blots were developed using an enhanced chemiluminescence (ECL) detection system (GE Healthcare, Buckinghamshire, United Kingdom).

Quantification and Subtyping of Haptoglobin

The concentration of plasma or serum haptoglobin was measured using an automated immunonephelometry BN-II system (Siemens Healthcare Diagnostics, Tokyo, Japan). The phenotype of haptoglobin α-chain was determined by nondenaturing (native) SDS-PAGE.[25]

Categorization of Hematologic Toxicities

Overall severity of hematologic toxicities after gemcitabine treatment was classified into categories I to IV based on the worst CTCAE grades of neutropenia and thrombocytopenia (Appendix Fig A1, online only), as follows: category I, grade 0 to 1 neutropenia and grade 0 thrombocytopenia; category II, grade 2 neutropenia or grade 1 thrombocytopenia; category III, grade 3 neutropenia or grade 2 thrombocytopenia; and category IV, grade 4 neutropenia or grade 3 to 4 thrombocytopenia.

Statistical Analysis

Statistical significance of intergroup differences was assessed using the Welch t test, χ^2 test, Wilcoxon test, or Kruskal-Wallis test, as appropriate. Multivariate regression analysis was performed using ordinal logistic regression modeling. Factors included in the prediction model were selected with a forward stepwise selection procedure using Akaike's Information Criterion (AIC). To correct biased sample sizes of categories, each observation was weighted according to the sample size of its category in the fitting process. The significance of differences between models with and without haptoglobin was assessed with the likelihood ratio test. Statistical analyses were performed using

an open-source statistical language R (version 2.7.0; http://www.r-project.org/) with the optional module design package.

RESULTS

Plasma Proteins Associated With Hematologic AEs

To identify a biomarker that can predict the occurrence of hematologic AEs associated with gemcitabine treatment, we compared the baseline plasma proteome between 25 patients who developed severe AEs (grade 3 to 4 neutropenia and/or grade 2 to 4 thrombocytopenia) and 22 patients who did not (grade 0) using 2DICAL. These levels of hematologic AEs have been used as criteria for dose reduction or postponement of gemcitabine-based treatments.[26-28] There was no significant difference in age, sex, Eastern Cooperative Oncology Group performance status, routine biochemical laboratory data, or pharmacokinetics of gemcitabine[15] (Table 1 and data not shown) between the two extreme groups of patients who were selected from cohort M0, but the patients who experienced severe AEs had significantly lower baseline peripheral-blood leukocyte, neutrophil, and platelet counts than patients without AEs (Table 1).

Among a total of 60,888 independent MS peaks detected within the range of 250 to 1,600 m/z and within the time range 20 to 70 minutes, we found that the mean intensity of triplicates differed significantly in 757 peaks ($P < .001$, Welch t test). Figure 1A is a representative two-dimensional view of all the MS peaks displayed with m/z along the x-axis and the retention time of LC along the y-axis. The 757 MS peaks whose expression differed significantly between patients with severe AEs and patients without AEs are highlighted in red.

One hundred fifteen MS/MS spectra acquired from 200 peaks with the smallest P values were matched to 41 proteins in the database (Mascot score of > 15; Appendix Tables A4 and A5, online only). Notably, MS peaks including one that was decreased in patients with severe AEs with the highest statistical significance ($P = .0000282$; Fig 1B) most recurrently (six times) matched the amino acid sequences of the haptoglobin (*HP*) gene product (Appendix Fig A2, online only). Figure 2A shows the distribution of two representative haptoglobin-derived MS peaks (ID 2062 [at 491 m/z and 44.5 minutes] and ID 5681 [at 602 m/z and 47 minutes]) in patients with severe AEs and without AEs. The differential expression and identification of haptoglobin were confirmed by denaturing SDS-PAGE and immunoblotting (Fig 2B).

Correlation of Haptoglobin With the Degree of Hematologic Toxicities

The levels of haptoglobin in plasma or serum samples obtained from 305 patients with advanced pancreatic cancer before gemcitabine treatment were measured by immunonephelometry and compared with the occurrence and severity of hematologic AEs. Consistent with 2DICAL analysis, the plasma levels of haptoglobin were significantly lower in the 25 patients with severe AEs than in the 22 patients without AEs ($P = .0002$, Wilcoxon test; Table 1).

The plasma level of haptoglobin showed a significant correlation with the NCI-CTCAE grade of neutropenia ($P = .012$, Kruskal-Wallis test) and hematologic toxicity categories ($P = .001$) in the 166 patients of cohort M0 (Fig 3A and Appendix Table A1). The correlation of haptoglobin levels with the grades of neutropenia and thrombocytopenia as well as the toxicity categories was consistently observed in the

Table 1. Clinical and Laboratory Data of Patients Without AEs and With Severe AEs

Factor	Patients Without AEs (n = 22)	Patients With Severe AEs (n = 25)	P
Haptoglobin, mg/dL			.0002
Mean	286	155	
SD	130	59	
Haptoglobin phenotype, No. of patients			.705*
Hp 2-2	12	14	
Hp 2-1	8	7	
Hp 1-1	2	4	
Sex, No. of patients			.344*
Male	12	17	
Female	10	8	
Age, years			.616
Mean	64	63	
SD	8	8	
ECOG performance status, No. of patients			.862*
0	12	13	
1	10	12	
2	0	0	
Body-surface area, m^2			.733
Mean	1.51	1.53	
SD	0.20	0.18	
Prior therapy, No. of patients			.867*
None	19	22	
Chemoradiotherapy using FU for LAPC	3	3	
Leucocyte, $\times 10^3/\mu L$			.0002
Mean	7.4	4.8	
SD	2.8	1.4	
Absolute neutrophil count, $\times 10^3/\mu L$			.0002
Mean	5.3	3.0	
SD	2.4	1.1	
Platelet, $\times 10^4/\mu L$			< .0001
Mean	28	17	
SD	11	6	
Hemoglobin, g/dL			.806
Mean	12.1	11.9	
SD	1.4	1.4	
Albumin, g/dL			.131
Mean	3.6	3.7	
SD	0.4	0.3	
Creatinine, mg/dL			.931
Mean	0.72	0.70	
SD	0.25	0.17	
AST, U/L			.430
Mean	37	29	
SD	26	13	
ALT, U/L			.624
Mean	43	32	
SD	37	24	
ALP, U/L			.815
Mean	593	459	
SD	591	283	
Pharmacokinetic parameters of gemcitabine			
C_{max}, $\mu g/mL$			.594
Mean	24.02	23.21	
SD	7.18	6.68	
AUC, $h \cdot \mu g/mL$			.462
Mean	9.95	10.74	
SD	2.36	3.03	

NOTE. Kruskal-Wallis test was applied to assess differences of values.
Abbreviations: AE, adverse event; SD, standard deviation; ECOG, Eastern Cooperative Oncology Group; FU, fluorouracil; LAPC, locally advanced pancreatic cancer; ALP, alkaline phosphatase; C_{max}, peak concentration; AUC, area under the curve.
*Calculated using the χ^2 test.

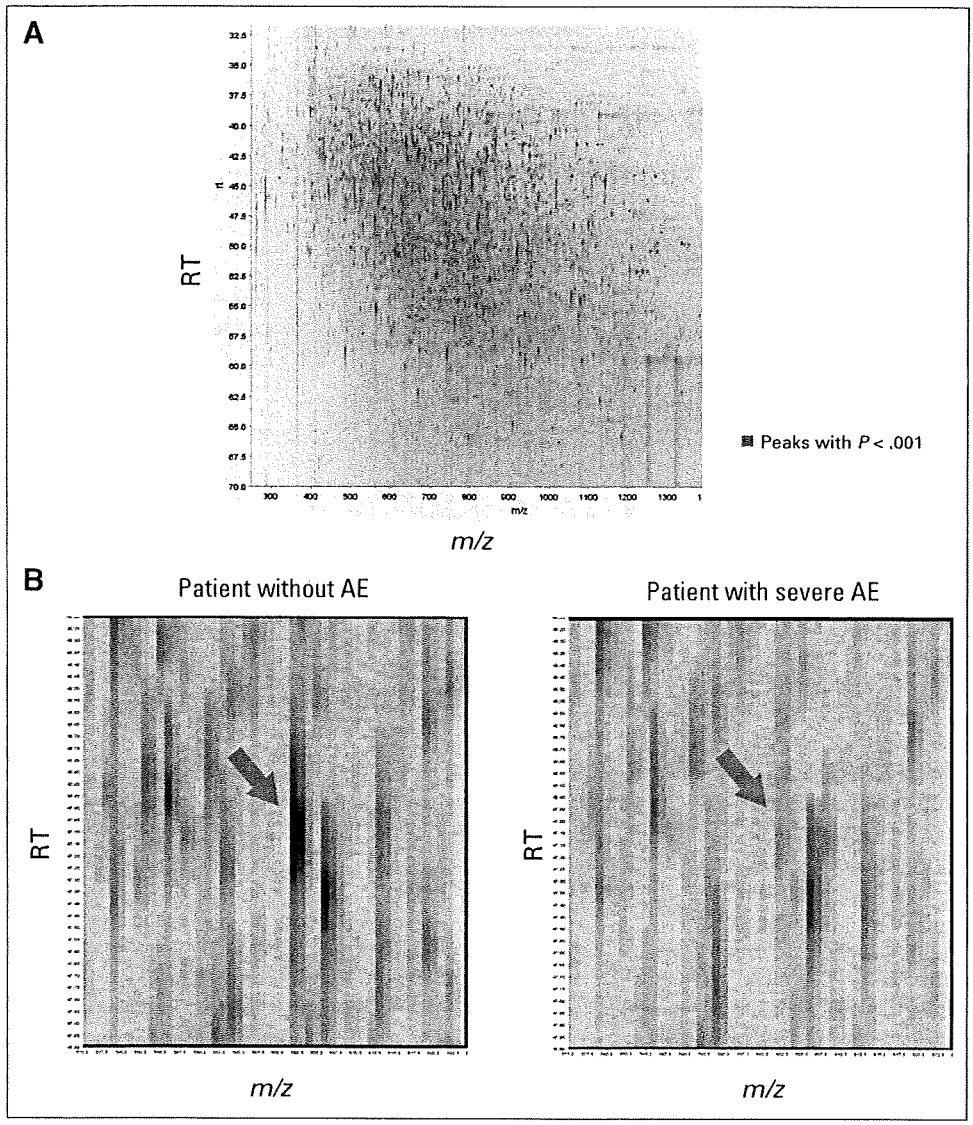

Fig 1. (A) Two-dimensional display of the entire (> 60,000) mass spectrometry (MS) peaks. The 757 MS peaks whose mean intensity differed significantly between patients with severe adverse events (AEs) and patients without AEs ($P < .001$, Welch t test) are highlighted in red. (B) MS peak with the smallest P value ($P = .0000282$; red arrows) in representative patients with severe AEs (right) and without AEs (left). RT, retention time.

two independent validation cohorts V1 (Fig 3B and Appendix Table A2) and V2 (Fig 3C and Appendix Table A3). The correlations between the levels of haptoglobin and the toxicity categories showed the highest statistical significance in all three cohorts (Figs 3A to 3C). The toxicity categories are criteria that we devised to evaluate the clinical severity of overall hematologic toxicities with emphasis on thrombocytopenia (Appendix Fig A1) from a practical viewpoint.[26-28] The management of neutropenia is largely uncomplicated because of the availability of granulocyte colony-stimulating factor.

Haptoglobin Phenotype and Hematologic Toxicities

Haptoglobin is a plasma protein that binds free hemoglobin and inhibits its oxidative activity. The human *HP* gene has two common polymorphic alleles (*H1* and *H2*), yielding individuals with the following three distinct phenotypes in the α-chain of haptoglobin protein: Hp 1-1, Hp 2-1, and Hp 2-2. The *H2* genotype has been reported to be associated with an increased risk of myocardial infarction and juvenile diabetes.[29] Although the frequency of the three phenotypes did not differ significantly with the severity of hematologic toxicities ($P > .360$, χ^2 test; Table 1 and Appendix Tables A1 to A3), the levels of haptoglobin were lower in individuals with the Hp 2-2 phenotype than in those with the Hp 2-1 or Hp 1-1 phenotype (Appendix Fig A3, online only).

Construction and Validation of a Model Predicting Hematologic Toxicities

In the M0 cohort (n = 166), 68 patients (41%) experienced category III hematologic toxicities, and 18 patients (11%) experienced category IV hematologic toxicities. Such levels of AE often necessitate the postponement of chemotherapy, and therefore, their prediction before drug administration is desirable. Because none of the parameters, including haptoglobin, was able to predict AEs satisfactorily when used individually (data not shown), we attempted to construct a multivariate predictive model to estimate the relative risk of suffering from hematologic toxicities of category III or worse. We searched for these parameters using a forward stepwise selection procedure by AIC

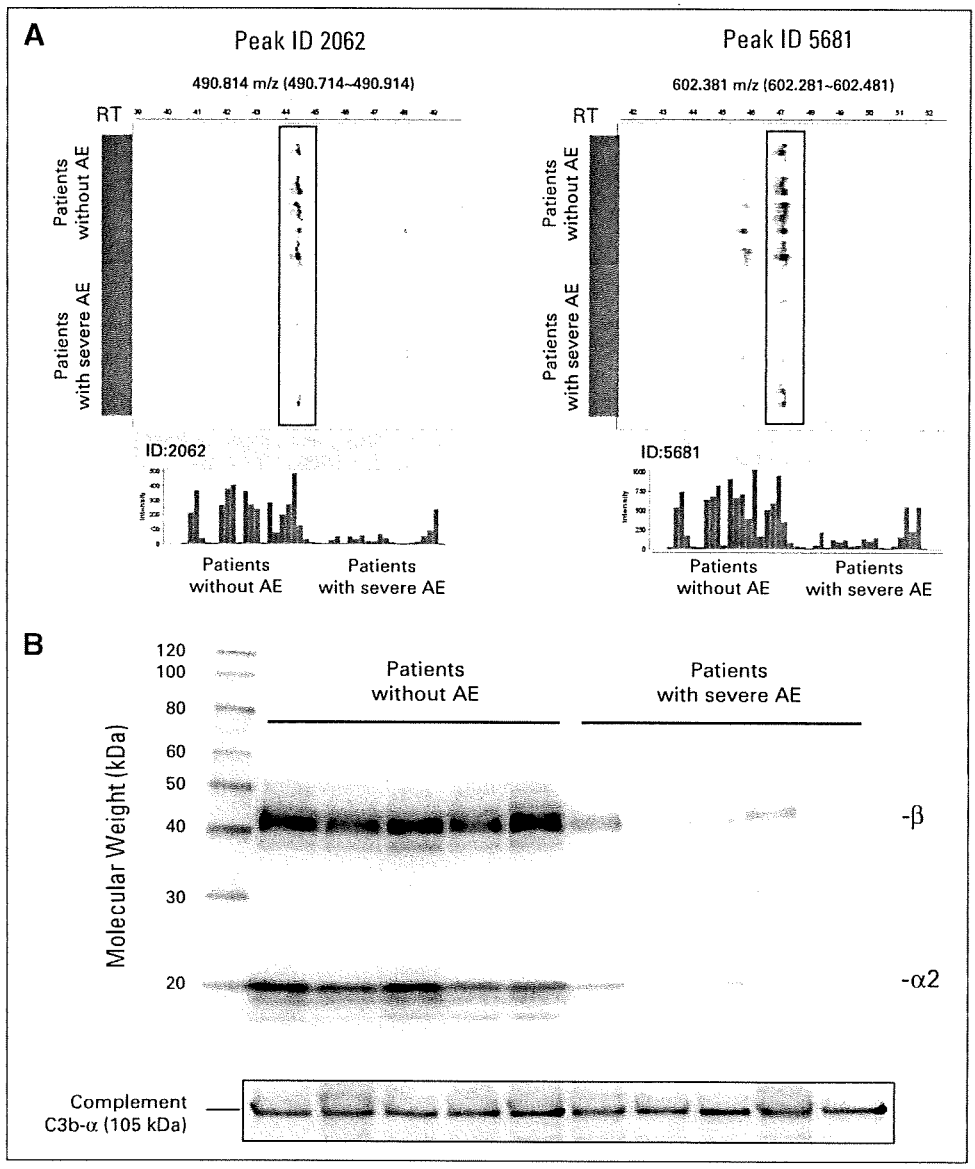

Fig 2. (A) Representative haptoglobin-derived mass spectrometry (MS) peaks in 47 triplicate liquid chromatography (LC)/MS runs (22 without adverse events [AEs], blue; and 25 with severe AEs, red) aligned along the retention time (RT) of LC (top). Columns represent the mean intensity of triplicates (bottom). (B) Detection of β- and α2-chains of haptoglobin and complement C3b-α (loading control) by immunoblotting.

from all of the clinical and laboratory data listed in Appendix Table A1 (available for 162 patients) and found that a combination of plasma haptoglobin level, haptoglobin phenotype, absolute neutrophil count (ANC), platelet count, and body-surface area (BSA) provided the lowest AIC value. The prediction model using this combination of parameters was significantly compromised when haptoglobin level and phenotype were excluded ($\chi^2 = 11.49$, $df = 3$, $P = .009$, likelihood ratio test). We estimated the independent contribution of each parameter to this prediction model and found that the baseline haptoglobin level was the second most important contributor to the model (Table 2).

On the basis of the results of multivariate logistic regression analysis, we constructed a nomogram in which the values of the five parameters (haptoglobin level, haptoglobin phenotype, ANC, platelet count, and BSA) are integrated into a single score (total point) to estimate the relative risk of having hematologic toxicities more severe than category II, category III, or category IV (Fig 4A). The area under the curve value for the prediction of categories III to IV was calculated to be 0.782 (95% CI, 0.711 to 0.843) in cohort M0 (Fig 4B). Predictive ability was confirmed in two independent validation cohorts, V1 and V2, that were not used for construction of the nomogram, with area under the curve values of 0.655 (95% CI, 0.546 to 0.754) and 0.747 (95% CI, 0.606 to 0.858), respectively (Fig 4B).

DISCUSSION

The early onset of severe AE necessitates dose reduction or postponement of treatment, leading to failure of chemotherapy.[30,31] In particular, the current gemcitabine monotherapy against advanced pancreatic cancer is mainly aimed at disease palliation, and thus, avoidance of life-threatening AEs is necessary. In this study, we first compared the plasma proteome of two groups of patients who showed distinct responses to the same protocol of gemcitabine therapy (Fig 1).

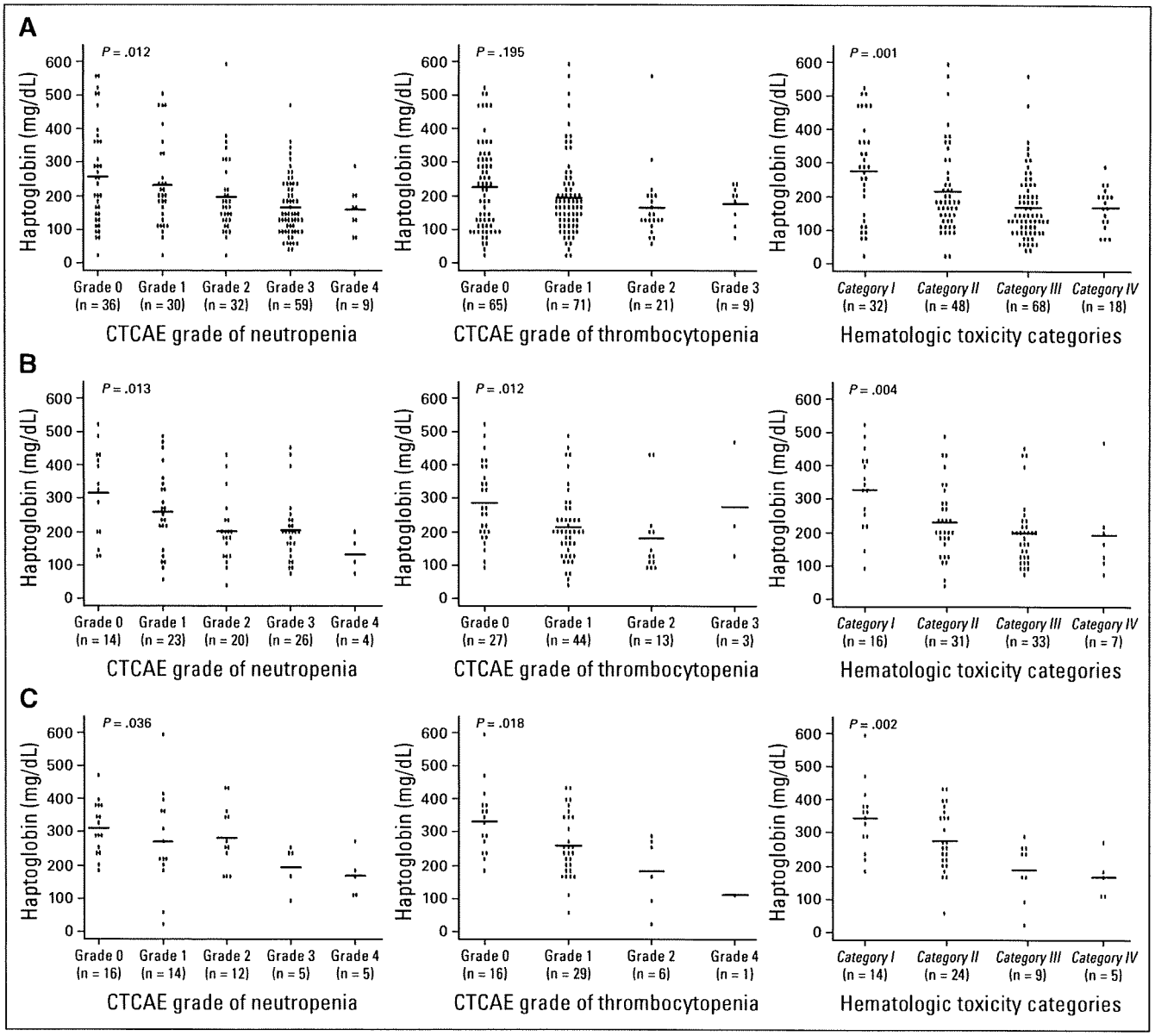

Fig 3. Plasma/serum haptoglobin levels according to the Common Terminology Criteria of Adverse Events (CTCAE; version 3.0). Grades of neutropenia (left), thrombocytopenia (middle), and hematologic toxicity categories (right) in the (A) modeling (M0), (B) validation-1 (V1), and (C) validation-2 (V2) cohorts. Horizontal lines represent the average levels of haptoglobin.

There was no significant difference in age distribution, Eastern Cooperative Oncology Group performance status, liver function, renal function, or prior chemoradiotherapy between the groups (Table 1 and data not shown), indicating that the occurrence of AEs does not merely reflect the general poor condition of patients but is based on certain biologic differences among individuals. We found that individuals who experienced severe AEs after administration of gemcitabine showed decreased baseline levels of plasma haptoglobin (Figs 1B and 2A), and this result was validated in three large cohorts using a different methodology (Fig 3 and Appendix Tables A1 to A3). Haptoglobin is an abundant plasma protein that usually cannot be measured by direct MS. However, constant depletion using an IgY-12 High Capacity Spin Column[32] allowed us to accentuate the differences in haptoglobin levels.

The molecular mechanisms that regulate the plasma haptoglobin level under physiologic and pathologic conditions are largely unknown. Haptoglobin is produced mainly in the liver, taken up by neutrophils, and stored within their cytoplasmic granules. Haptoglobin is released in response to a variety of stimuli, such as infection, trauma, and malignancy,[33] and modulates inflammatory responses. Tumor necrosis factor α induces the release of haptoglobin from neutrophils in vitro.[34] Interestingly, tumor necrosis factor α and its soluble receptors have been reported to be associated with an increased risk of hematologic toxicities.[12,35,36]

Table 2. Contribution of Parameters to Prediction of Hematologic Toxicities Associated With Gemcitabine

Factor	Odds Ratio*	95% CI	P
Haptoglobin level	0.71	0.53 to 0.97	.031†
Phenotype of haptoglobin (*v* Hp 2-2)			
Hp 2-1	0.61	0.31 to 1.21	.159
Hp 1-1	2.16	0.70 to 6.69	.180
Absolute neutrophil count	0.72	0.61 to 0.86	.0003†
Platelet count	0.63	0.39 to 1.01	.056
Body-surface area	3.86	0.63 to 23.76	.145

NOTE. A forward stepwise selection based on Akaike's Information Criterion was used to select parameters for multivariate analysis.
*Odds ratios are per 100 mg/dL increase for haptoglobin level, per 1,000/μL increase for absolute neutrophil count, per $10 \times 10^4/\mu$L increase for platelet, and per 1.00 m^2 increase for body-surface area.
†$P < .05$.

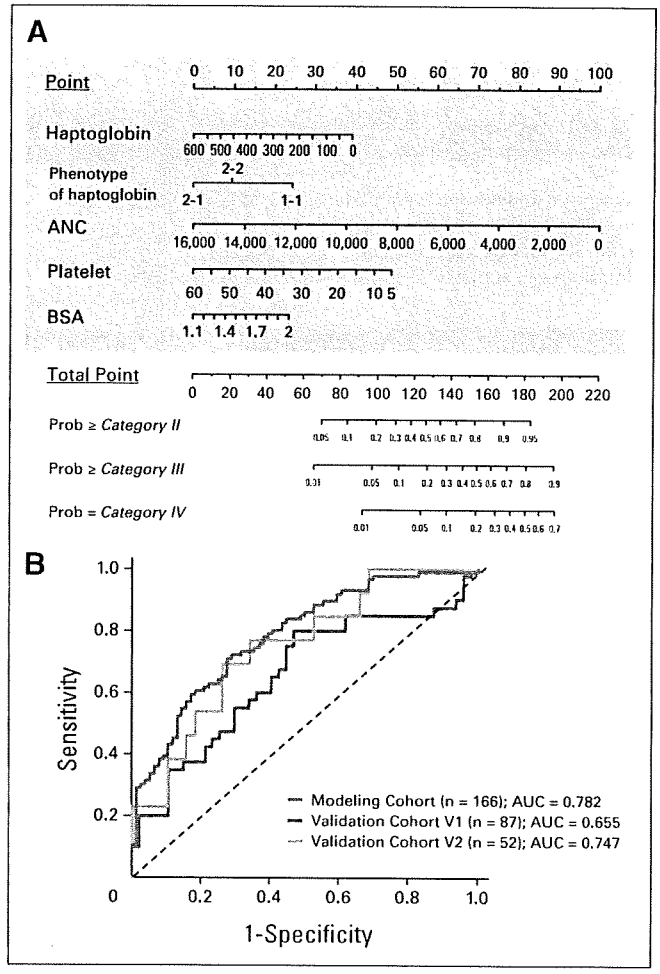

Fig 4. (A) Nomogram to estimate the risk of hematologic toxicities more severe than category II (top), category III (middle), and category IV (bottom). Please see Appendix Figure A4 and its legend for usage. (B) Receiver operating characteristic (ROC) analysis of nomogram for the prediction of category III and IV hematologic toxicities in the modeling (gray), validation-1 (V1; blue), and validation-2 (V2; gold) cohorts. ANC, absolute neutrophil count; BSA, body-surface area; AUC, area under the curve.

To derive clinical applicability from these basic findings, we constructed a model (nomogram) that estimates the possibility of occurrence of hematologic AE before administration of gemcitabine (Fig 4A and Appendix Fig A4). The significance of the model was further confirmed in two independent validation cohorts (Fig 4B). Although its accuracy was far from perfect, the model seems to be practically sufficient for identifying individuals who are likely to suffer from hematologic toxicities after administration of gemcitabine. Various cytotoxic or molecular targeting agents have been tested in combination with gemcitabine in phase III trials, but no apparent additional therapeutic benefit has been demonstrated.[5,6,9,10] The application of this model to patient selection may improve the outcome of such trials. We are now trying to identify new biomarkers that can predict the efficacy of gemcitabine treatment using a similar strategy.

The phenotypes of haptoglobin have been reported to be associated with different hemoglobin-binding, antioxidative, and prostaglandin synthesis–initiating activities.[33] Although haptoglobin phenotype was not significantly associated with hematologic toxicities (Table 1 and Appendix Tables A1 to A3), the average levels of haptoglobin differed among individuals with different phenotypes (Appendix Fig A3), as described previously.[33] For this reason, haptoglobin phenotype was selected in the prediction model by AIC analysis (Table 2). BSA has been repeatedly selected as one of the multivariate parameters for predicting the AEs of anticancer therapies in other studies,[14,37] suggesting a potential lack of accuracy in calculating individually optimized drug dose based solely on BSA, as pointed out previously.[38,39]

In conclusion, we have revealed that a decreased level of haptoglobin is the second most significant factor predicting hematologic toxicities associated with gemcitabine monotherapy after ANC (Table 2). Measurement of haptoglobin is now established as a laboratory test and could be readily incorporated into routine oncologic practice. However, the predictive significance of haptoglobin was revealed only in a retrospective population from a single institution and must, therefore, be validated in an independent prospective multi-institutional study. It was not determined in this study whether haptoglobin could be a predictive biomarker for the AEs of other chemotherapeutic agents. To improve the accuracy of prediction, the discovery of new biomarkers with higher specificity and sensitivity will be necessary. While bearing all these limitations in mind, the present findings may provide novel insights not only into the molecular mechanisms by which gemcitabine causes hematologic toxicities, but also into new avenues for the development of new chemotherapeutic agents with lower toxicity.

AUTHORS' DISCLOSURES OF POTENTIAL CONFLICTS OF INTEREST

Although all authors completed the disclosure declaration, the following author(s) indicated a financial or other interest that is relevant to the subject matter under consideration in this article. Certain relationships marked with a "U" are those for which no compensation was received; those relationships marked with a "C" were compensated. For a detailed description of the disclosure categories, or for more information about ASCO's conflict of interest policy, please refer to the Author Disclosure Declaration and the Disclosures of Potential Conflicts of Interest section in Information for Contributors.

Employment or Leadership Position: None **Consultant or Advisory Role:** None **Stock Ownership:** None **Honoraria:** Nagahiro Saijo, Elli

Lilly **Research Funding:** Nagahiro Saijo, National Institute of Biomedical Innovation **Expert Testimony:** None **Other Remuneration:** None

AUTHOR CONTRIBUTIONS

Conception and design: Junichi Matsubara, Masaya Ono, Setsuo Hirohashi, Tesshi Yamada
Financial support: Nagahiro Saijo, Tesshi Yamada
Administrative support: Tsutomu Chiba, Setsuo Hirohashi
Provision of study materials or patients: Hideki Ueno, Takuji Okusaka, Junji Furuse, Koh Furuta, Emiko Sugiyama, Yoshiro Saito, Nahoko Kaniwa, Junichi Sawada
Collection and assembly of data: Junichi Matsubara, Ayako Negishi, Kazufumi Honda, Nagahiro Saijo, Tesshi Yamada
Data analysis and interpretation: Junichi Matsubara, Masaya Ono, Tomohiro Sakuma
Manuscript writing: Junichi Matsubara, Tesshi Yamada
Final approval of manuscript: Junichi Matsubara, Masaya Ono, Junichi Sawada, Tsutomu Chiba, Nagahiro Saijo, Setsuo Hirohashi, Tesshi Yamada

REFERENCES

1. Honda K, Hayashida Y, Umaki T, et al: Possible detection of pancreatic cancer by plasma protein profiling. Cancer Res 65:10613-10622, 2005
2. Ministry of Health, Labour and Welfare: Japanese Government: Statistical Database 2007. http://wwwdbtk.mhlw.go.jp/toukei/youran/data19k/1-31.xls
3. American Cancer Society: Cancer Facts and Figures 2007. Atlanta, GA: American Cancer Society, 2007
4. Burris HA 3rd, Moore MJ, Andersen J, et al: Improvements in survival and clinical benefit with gemcitabine as first-line therapy for patients with advanced pancreas cancer: A randomized trial. J Clin Oncol 15:2403-2413, 1997
5. Louvet C, Labianca R, Hammel P, et al: Gemcitabine in combination with oxaliplatin compared with gemcitabine alone in locally advanced or metastatic pancreatic cancer: Results of a GERCOR and GISCAD phase III trial. J Clin Oncol 23:3509-3516, 2005
6. Herrmann R, Bodoky G, Ruhstaller T, et al: Gemcitabine plus capecitabine compared with gemcitabine alone in advanced pancreatic cancer: A randomized, multicenter, phase III trial of the Swiss Group for Clinical Cancer Research and the Central European Cooperative Oncology Group. J Clin Oncol 25:2212-2217, 2007
7. National Comprehensive Cancer Network: Clinical Practice Guidelines in Oncology: Pancreatic Adenocarcinoma V. 1. 2008. http://www.nccn.org/professionals/physician_gls/PDF/pancreatic.pdf
8. Casper ES, Green MR, Kelsen DP, et al: Phase II trial of gemcitabine (2,2'-difluorodeoxycytidine) in patients with adenocarcinoma of the pancreas. Invest New Drugs 12:29-34, 1994
9. Kindler HL, Niedzwiecki D, Hollis D, et al: A double-blind, placebo-controlled, randomized phase III trial of gemcitabine (G) plus bevacizumab (B) versus gemcitabine plus placebo (P) in patients (pts) with advanced pancreatic cancer (PC): A preliminary analysis of Cancer and Leukemia Group B (CALGB). J Clin Oncol 25:199s, 2007 (suppl; abstr 4508)
10. Philip PA, Benedetti J, Fenoglio-Preiser C, et al: Phase III study of gemcitabine (G) plus cetuximab versus gemcitabine (C) in patients (pts) with locally advanced or metastatic pancreatic adenocarcinoma (Pca): SWOG S0205 study. J Clin Oncol 25:199s, 2007 (suppl; abstr LBA4509)
11. Ziepert M, Schmits R, Trumper L, et al: Prognostic factors for hematotoxicity of chemotherapy in aggressive non-Hodgkin's lymphoma. Ann Oncol 19:752-762, 2008
12. Voog E, Bienvenu J, Warzocha K, et al: Factors that predict chemotherapy-induced myelosuppression in lymphoma patients: Role of the tumor necrosis factor ligand-receptor system. J Clin Oncol 18:325-331, 2000
13. Pond GR, Siu LL, Moore M, et al: Nomograms to predict serious adverse events in phase II clinical trials of molecularly targeted agents. J Clin Oncol 26:1324-1330, 2008
14. Aslani A, Smith RC, Allen BJ, et al: The predictive value of body protein for chemotherapy-induced toxicity. Cancer 88:796-803, 2000
15. Sugiyama E, Kaniwa N, Kim SR, et al: Pharmacokinetics of gemcitabine in Japanese cancer patients: The impact of a cytidine deaminase polymorphism. J Clin Oncol 25:32-42, 2007
16. Yonemori K, Ueno H, Okusaka T, et al: Severe drug toxicity associated with a single-nucleotide polymorphism of the cytidine deaminase gene in a Japanese cancer patient treated with gemcitabine plus cisplatin. Clin Cancer Res 11:2620-2624, 2005
17. Hanash S: Disease proteomics. Nature 422: 226-232, 2003
18. Yamaguchi U, Nakayama R, Honda K, et al: Distinct gene expression-defined classes of gastrointestinal stromal tumor. J Clin Oncol 26:4100-4108, 2008
19. Taguchi F, Solomon B, Gregorc V, et al: Mass spectrometry to classify non-small-cell lung cancer patients for clinical outcome after treatment with epidermal growth factor receptor tyrosine kinase inhibitors: A multicohort cross-institutional study. J Natl Cancer Inst 99:838-846, 2007
20. Yanagisawa K, Tomida S, Shimada Y, et al: A 25-signal proteomic signature and outcome for patients with resected non-small-cell lung cancer. J Natl Cancer Inst 99:858-867, 2007
21. Ono M, Shitashige M, Honda K, et al: Label-free quantitative proteomics using large peptide data sets generated by nanoflow liquid chromatography and mass spectrometry. Mol Cell Proteomics 5:1338-1347, 2006
22. General Rules for the Study of Pancreatic Cancer (ed 5). Tokyo, Japan Japanese Pancreas Society
23. Honda K, Yamada T, Hayashida Y, et al: Actinin-4 increases cell motility and promotes lymph node metastasis of colorectal cancer. Gastroenterology 128:51-62, 2005
24. Idogawa M, Yamada T, Honda K, et al: Poly(ADP-ribose) polymerase-1 is a component of the oncogenic T-cell factor-4/beta-catenin complex. Gastroenterology 128:1919-1936, 2005
25. Tolson J, Bogumil R, Brunst E, et al: Serum protein profiling by SELDI mass spectrometry: Detection of multiple variants of serum amyloid alpha in renal cancer patients. Lab Invest 84:845-856, 2004
26. Tempero M, Plunkett W, Ruiz Van Haperen V, et al: Randomized phase II comparison of dose-intense gemcitabine: Thirty-minute infusion and fixed dose rate infusion in patients with pancreatic adenocarcinoma. J Clin Oncol 21:3402-3408, 2003
27. Kindler HL, Friberg G, Singh DA, et al: Phase II trial of bevacizumab plus gemcitabine in patients with advanced pancreatic cancer. J Clin Oncol 23: 8033-8040, 2005
28. Cascinu S, Berardi R, Labianca R, et al: Cetuximab plus gemcitabine and cisplatin compared with gemcitabine and cisplatin alone in patients with advanced pancreatic cancer: A randomised, multicentre, phase II trial. Lancet Oncol 9:39-44, 2008
29. Shindo S: Haptoglobin subtyping with anti-haptoglobin alpha chain antibodies. Electrophoresis 11:483-488, 1990
30. Hryniuk W, Bush H: The importance of dose intensity in chemotherapy of metastatic breast cancer. J Clin Oncol 2:1281-1288, 1984
31. Levin L, Hryniuk WM: Dose intensity analysis of chemotherapy regimens in ovarian carcinoma. J Clin Oncol 5:756-767, 1987
32. Huang L, Harvie G, Feitelson JS, et al: Immunoaffinity separation of plasma proteins by IgY microbeads: Meeting the needs of proteomic sample preparation and analysis. Proteomics 5:3314-3328, 2005
33. Langlois MR, Delanghe JR: Biological and clinical significance of haptoglobin polymorphism in humans. Clin Chem 42:1589-1600, 1996
34. Berkova N, Gilbert C, Goupil S, et al: TNF-induced haptoglobin release from human neutrophils: Pivotal role of the TNF p55 receptor. J Immunol 162:6226-6232, 1999
35. Petros WP, Rabinowitz J, Gibbs JP, et al: Effect of plasma TNF-alpha on filgrastim-stimulated hematopoiesis in mice and humans. Pharmacotherapy 18:816-823, 1998
36. Holler E, Kolb HJ, Moller A, et al: Increased serum levels of tumor necrosis factor alpha precede major complications of bone marrow transplantation. Blood 75:1011-1016, 1990
37. Shayne M, Culakova E, Poniewierski MS, et al: Dose intensity and hematologic toxicity in older cancer patients receiving systemic chemotherapy. Cancer 110:1611-1620, 2007
38. Ratain MJ: Body-surface area as a basis for dosing of anticancer agents: Science, myth, or habit? J Clin Oncol 16:2297-2298, 1998
39. Gurney H: Dose calculation of anticancer drugs: A review of the current practice and introduction of an alternative. J Clin Oncol 14:2590-2611, 1996

Acknowledgment

We thank Ayako Igarashi and Yuka Nakamura for their technical assistance.

mTOR Signal and Hypoxia-Inducible Factor-1α Regulate CD133 Expression in Cancer Cells

Kazuko Matsumoto,[1] Tokuzo Arao,[1] Kaoru Tanaka,[1] Hiroyasu Kaneda,[1] Kanae Kudo,[1] Yoshihiko Fujita,[1] Daisuke Tamura,[1] Keiichi Aomatsu,[1] Tomohide Tamura,[3] Yasuhide Yamada,[3] Nagahiro Saijo,[2] and Kazuto Nishio[1]

[1]Department of Genome Biology, [2]Kinki University School of Medicine, Osaka-Sayama, Osaka, Japan; and [3]Department of Medical Oncology, National Cancer Center Hospital, Chuo-ku, Tokyo, Japan

Abstract

The underlying mechanism regulating the expression of the cancer stem cell/tumor-initiating cell marker CD133/prominin-1 in cancer cells remains largely unclear, although knowledge of this mechanism would likely provide important biological information regarding cancer stem cells. Here, we found that the inhibition of mTOR signaling up-regulated CD133 expression at both the mRNA and protein levels in a CD133-overexpressing cancer cell line. This effect was canceled by a rapamycin-competitor, tacrolimus, and was not modified by conventional cytotoxic drugs. We hypothesized that hypoxia-inducible factor-1α (HIF-1α), a downstream molecule in the mTOR signaling pathway, might regulate CD133 expression; we therefore investigated the relation between CD133 and HIF-1α. Hypoxic conditions up-regulated HIF-1α expression and inversely down-regulated CD133 expression at both the mRNA and protein levels. Similarly, the HIF-1α activator deferoxamine mesylate dose-dependently down-regulated CD133 expression, consistent with the effects of hypoxic conditions. Finally, the correlations between CD133 and the expressions of HIF-1α and HIF-1β were examined using clinical gastric cancer samples. A strong inverse correlation ($r = -0.68$) was observed between CD133 and HIF-1α, but not between CD133 and HIF-1β. In conclusion, these results indicate that HIF-1α down-regulates CD133 expression and suggest that mTOR signaling is involved in the expression of CD133 in cancer cells. Our findings provide a novel insight into the regulatory mechanisms of CD133 expression via mTOR signaling and HIF-1α in cancer cells and might lead to insights into the involvement of the mTOR signal and oxygen-sensitive intracellular pathways in the maintenance of stemness in cancer stem cells. [Cancer Res 2009;69(18):7160–4]

Introduction

The CD133/prominin-1 protein is a five-transmembrane molecule expressed on the cell surface that is widely regarded as a stem cell marker. Growing evidence indicates that CD133 can be used as a cell marker for cancer stem cells or tumor-initiating cells in colon cancer, prostate cancer, pancreatic cancer, hepatocellular carcinoma, neural tumors, and renal cancer (1). Strict regulatory mechanisms governing CD133 expression are thought to be deeply related to inherent cancer stemness; however, such mechanisms remain largely unclear, especially in cancer cells. In brain tumors, the Hedgehog (2), bone morphogenetic protein (3), and Notch (4) signaling pathways have been implicated in the control of CD133+ cancer stem cell function.

Some investigators have shown a relation between hypoxia and CD133 expression in brain tissue. The percentage of CD133-expressing cells was found to increase in a glioma cell line cultured under hypoxic conditions (5), and mouse fetal cortical precursors cultured under normoxic conditions exhibited a reduction in CD133(hi)CD24(lo) multipotent precursors and the failure of the remaining CD133(hi)CD24(lo) cells to generate glia (6). With the exception of these studies in brain tissue, however, data on the expression of CD133 and the involvement of hypoxia and other signaling pathways in cancer cells remains limited.

Several reports have indicated that mTOR is a positive regulator of hypoxia-inducible factor (HIF) expression and activity (7), and the inhibition of HIF-mediated gene expression is considered to be related to the antitumor activity of mTOR inhibitors in renal cell carcinoma (8). We found that mTOR signaling was involved in CD133 expression in gastric and colorectal cancer cells. Thus, we investigated the regulatory mechanism of CD133 in cancer cells.

Materials and Methods

Reagents. 5-Fluorouracil, irinotecan (CPT-11), and rapamycin were purchased from Sigma-Aldrich. Gemcitabine was provided by Eli Lilly. Tacrolimus (LKT Laboratories), LY294002 and wortmannin (Cell Signaling Technology), and deferoxamine mesylate (DFO; Sigma-Aldrich) were purchased from the indicated companies.

Cell cultures and hypoxic conditions. All of the 28 cell lines used in this study were maintained in RPMI 1640 (Sigma) supplemented with 10% heat-inactivated fetal bovine serum (Life Technologies), except for LoVo (F12; Nissui Pharmaceutical), WiDr, IM95, and HEK293 (DMEM; Nissui Pharmaceutical), and Huvec (Humedia; Kurabo). Hypoxic conditions (0.1% O_2) were achieved using the AnaeroPouch-Anaero (Mitsubishi Gas Chemical) with monitoring using an oxygen indicator.

Real-time reverse transcription-PCR. The methods were previously described (9). The primers used for the real-time reverse transcription-PCR (RT-PCR) were as follows: CD133, forward 5′-AGT GGC ATC GTG CAA ACC TG-3′ and reverse 5′-CTC CGA ATC CAT TCG ACG ATA GTA-3′; glyceraldehyde-3-phosphate dehydrogenase (GAPD), forward 5′-GCA CCG TCA AGG CTG AGA AC-3′ and reverse 5′-ATG GTG GTG AAG ACG CCA GT-3′. GAPD was used to normalize the expression levels in the subsequent quantitative analyses.

Clinical samples. The mRNA expression levels of CD133, HIF-1α, and HIF-1β in gastric cancer specimens were obtained from previously published microarray data (9).

Note: Supplementary data for this article are available at Cancer Research Online (http://cancerres.aacrjournals.org/).

K. Matsumoto and T. Arao contributed equally to this work.

Requests for reprints: Kazuto Nishio, Department of Genome Biology, Kinki University School of Medicine, 377-2 Ohno-higashi, Osaka-Sayama, Osaka 589-8511, Japan. Phone: 81-72-366-0221; Fax: 81-72-366-0206; E-mail: knishio@med.kindai.ac.jp.

doi:10.1158/0008-5472.CAN-09-1289

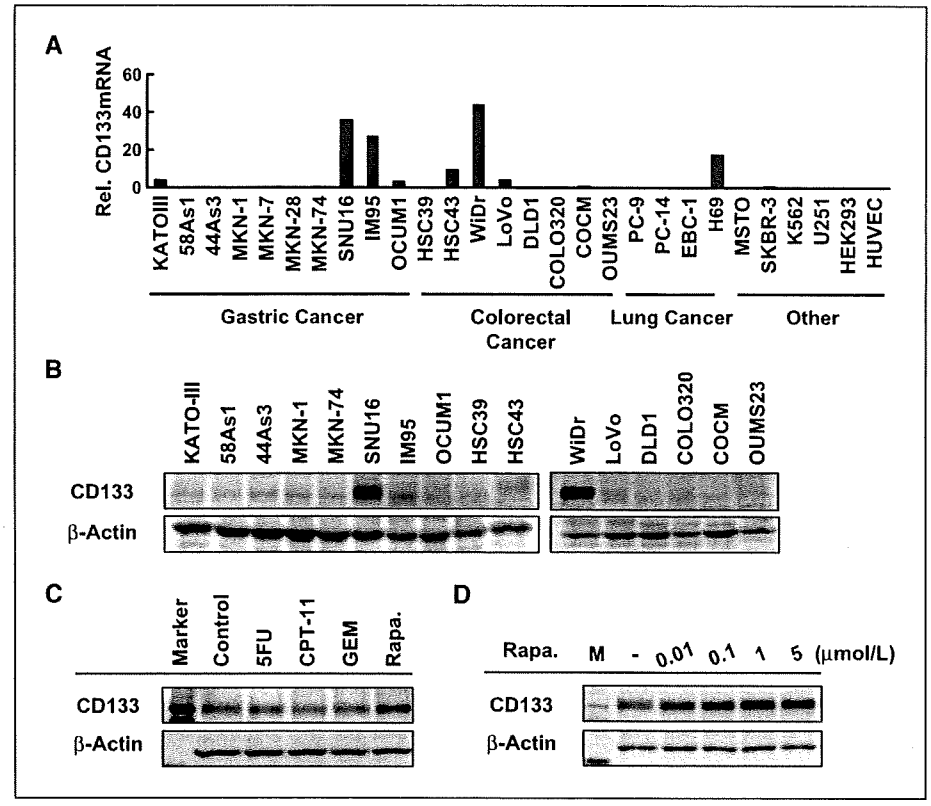

Figure 1. Rapamycin up-regulates CD133 expression. *A*, the mRNA expression levels of CD133 were examined using real-time RT-PCR in 26 cancer cell lines. *B*, the protein expressions of CD133 were determined using Western blotting in 16 gastric and colorectal cancer cell lines. *C*, Western blot of CD133 expression in WiDr cells exposed to cytotoxic drugs [1 μmol/L of 5-fluorouracil (*5-FU*), CPT-11, and gemcitabine (*GEM*)] and rapamycin (1 μmol/L) for 48 h. Note that only rapamycin up-regulates CD133 expression. *D*, WiDr cells were exposed to rapamycin at the indicated concentrations (0, 0.01, 0.1, 1, and 5 μmol/L) for 48 h. Rapamycin dose-dependently up-regulated CD133 expression. *Rel. CD133 mRNA*, normalized mRNA expression levels (CD133/GAPD × 10^4); *Rapa.*, rapamycin.

Immunoblotting. A Western blot analysis was performed as described previously (10). The experiment was performed in triplicate. The following antibodies were used: monoclonal CD133 antibody (W6B3C1; Miltenyi Biotec), rabbit polyclonal HIF-1α antibody (Novus Biologicals, Inc.), β-actin antibody, and HRP-conjugated secondary antibody (Cell Signaling Technology).

Results

Inhibition of the mTOR signal up-regulates CD133 expression in CD133-overexpressing gastrointestinal cancer cells. We examined the mRNA expression levels of CD133 in 26 cancer cell

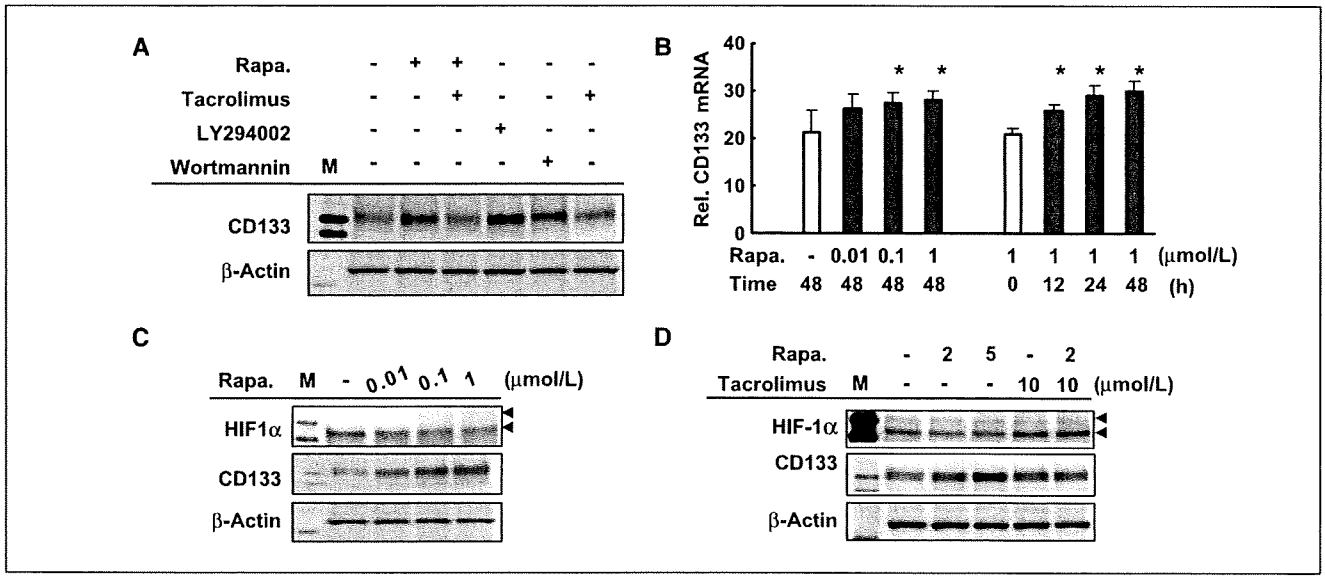

Figure 2. Rapamycin down-regulates HIF-1α expression and up-regulates CD133 expression at the transcriptional level. *A*, WiDr cells were exposed to rapamycin, the rapamycin-competitor tacrolimus, and the phosphoinositide-3-kinase inhibitors LY294002 and wortmannin for 48 h at concentrations of 10 μmol/L. The inhibition of mTOR signaling up-regulated CD133 expression. *B*, rapamycin up-regulated the expression of CD133 mRNA in WiDr cells in a time-dependent and dose-dependent manner. *Columns*, mean determined using real-time RT-PCR; *bars*, SD. *C* and *D*, rapamycin exposure and HIF-1α expression. WiDr cells were exposed to rapamycin with/without tacrolimus at the indicated concentration for 48 h. Rapamycin down-regulated HIF-1α expression and inversely up-regulated CD133 expression; these effects were canceled by tacrolimus. *Rel. CD133 mRNA*, normalized mRNA expression levels (CD133/GAPD × 10^4); *Rapa.*, rapamycin.

lines using real-time RT-PCR. Several gastric, colorectal, and lung cancer cell lines such as SNU16, IM95, HSC43, WiDr, and H69, overexpressed CD133 (Fig. 1*A*). The increased expression of CD133 protein was also confirmed in these cell lines (Fig. 1*B*). The mTOR inhibitor rapamycin, but not cytotoxic drugs (5-fluorouracil, CPT-11, and gemcitabine), increased the expression of CD133 in a dose-dependent manner in CD133-overexpressing WiDr cells (Fig. 1*C* and *D*). These results indicate that mTOR signaling is involved in the expression of CD133 in cancer cells.

Rapamycin down-regulated HIF-1α expression and up-regulated CD133 expression at the transcriptional level. To examine the signal transduction of rapamycin-induced CD133 expression, we used the rapamycin-competitor tacrolimus and the phosphoinositide-3-kinase inhibitors LY294002 and wortmannin. Tacrolimus (10 μmol/L) completely canceled the up-regulation of CD133 induced by rapamycin. The inhibition of phosphoinositide-3-kinase by LY294002 (10 μmol/L) and wortmannin (10 μmol/L) also up-regulated CD133 expression (Fig. 2*A*). Rapamycin up-regulated CD133 expression at the transcriptional level in a dose-dependent and time-dependent manner (Fig. 2*B*).

The inhibition of mTOR signaling is likely to lead to the down-regulation of the expression of certain molecules because the mTOR complex positively regulates the general translational machinery. Under the inhibition of mTOR signaling, HIF-1α, among several downstream molecules of mTOR, can activate transcription by acting as a repressor of specific transcription factors such as the MYC-associated protein X homodimer (11). Therefore, we focused on the possible role of HIF-1α in the regulation of CD133 expression. Rapamycin down-regulated HIF-1α expression but up-regulated CD133 expression (Fig. 2*C*). Meanwhile, tacrolimus canceled the effect of rapamycin on the expressions of HIF-1α and CD133 (Fig. 2*D*). These results suggest that the down-regulation of HIF-1α may mediate the up-regulation of CD133 expression in cancer cells. Up-regulation of CD133 expression by rapamycin was reproducibly observed in the CD133 high-expressing cell lines, but not in CD133 low-expressing cell lines (Supplemental Fig. S2).

Induction of HIF-1α down-regulates CD133 expression in cancer cells. Hypoxia mediates the stabilization of HIF-1α protein and enables its escape from rapid degradation, facilitating the up-regulation of HIF-1α expression (12). Hypoxia strongly induced HIF-1α expression, whereas CD133 expression was down-regulated in all three CD133-overexpressing cell lines (Fig. 3*A*). Rapamycin dose-dependently up-regulated CD133 expression under normoxic conditions, but no effect was seen under hypoxic conditions. We speculated that the effect of hypoxia on the induction of HIF-1α is much higher than the effect of rapamycin on the down-regulation of HIF-1α. The expression of CD133 mRNA was also strongly down-regulated under hypoxic conditions in all three cell lines (Fig. 3*B*) and in three additional cell lines (Supplemental Fig. S1).

In addition, DFO, a known HIF-1α activator, induced HIF-1α expression in a dose-dependent manner but down-regulated the expression of CD133 at both the mRNA and protein levels in WiDr cells (Fig. 3*C* and *D*), and in three additional cell lines (Supplemental Fig. S2). These results were consistent with those obtained under hypoxic conditions. Both hypoxia and DFO exposure markedly down-regulated CD133 expression, strongly suggesting that induction of HIF-1α results in the down-regulation of CD133 expression.

Inverse correlation between CD133 and HIF-1α in clinical samples. Finally, to address whether CD133 and HIF-1α expression are inversely correlated in clinical samples of gastric cancer

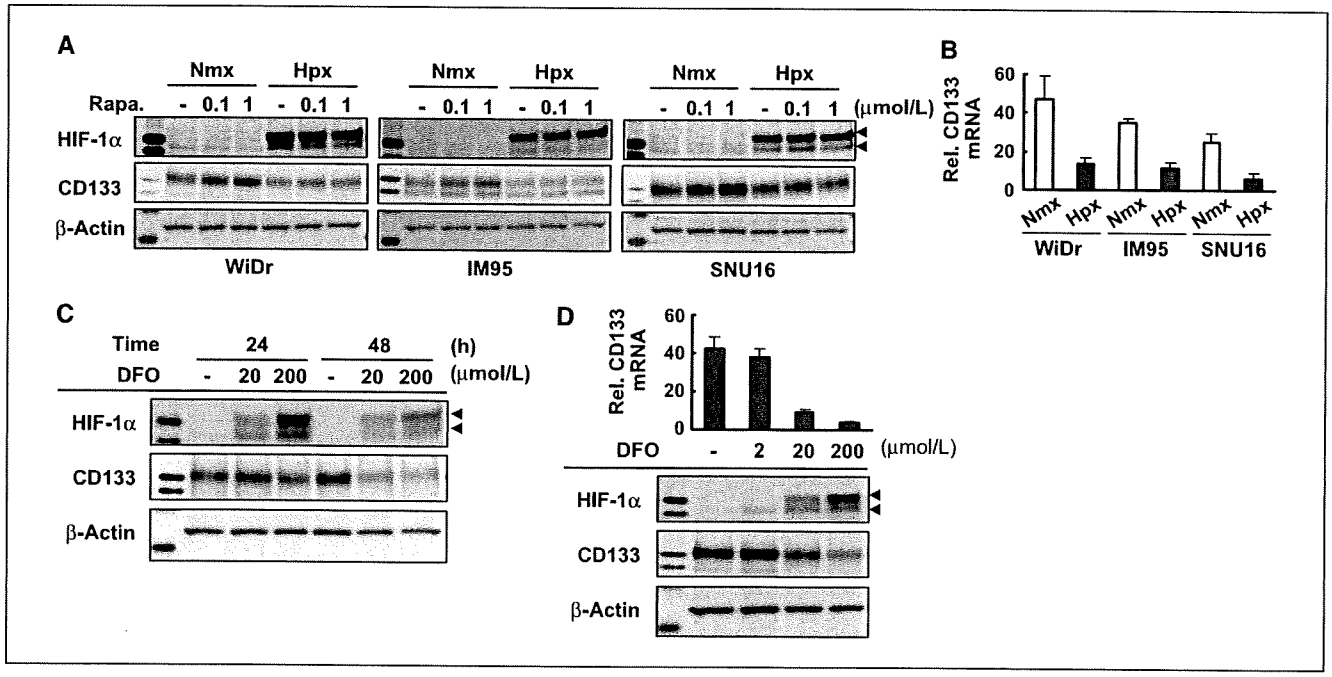

Figure 3. Induction of HIF-1α down-regulates CD133 expression in cancer cells. *A*, three gastrointestinal cancer cell lines were exposed to rapamycin under normoxic or hypoxic conditions for 24 h. Hypoxia induced HIF-1α expression and inversely down-regulated CD133 expression. *B*, hypoxia strongly down-regulated CD133 expression at the mRNA level. *Columns*, mean determined using real-time RT-PCR; *bars*, SD. *C*, DFO, a known HIF-1α activator, induced HIF-1α expression and down-regulated CD133 expression in WiDr cells. *D*, DFO induced these effects at both the mRNA and protein levels. Note that both hypoxia and DFO exposure had similar effects on HIF-1α induction and CD133 down-regulation. *Rel. CD133 mRNA*, normalized mRNA expression levels (CD133/GAPD × 10^4); *Rapa.*, rapamycin.

specimens, we examined the expression of these molecules using previously published microarray data (9). The expressions of CD133 and HIF-1α were inversely correlated in gastric cancer ($r = -0.68$; Fig. 4*A*), whereas the expressions of CD133 and HIF-1β were not ($r = -0.05$; Fig. 4*A*). These results are consistent with the *in vitro* findings in the present study.

Taken together, the present results suggest that an oxygen-sensitive intracellular pathway involving both HIF-1α and mTOR signaling may, at least in part, regulate CD133 expression in cancer cells (shown in the schema in Fig. 4*B*).

Discussion

Hypoxic conditions promote the proliferation of mammalian ES cells more efficiently than normoxia and are thought to be required for the maintenance of full pluripotency. Hematopoietic stem cells are located in the bone marrow, which is a physiologically hypoxic environment, and the survival and/or self-renewal of hematopoietic stem cells is enhanced *in vitro* if the cells are cultured under hypoxic conditions (13). Thus, accumulating data indicates that oxygen levels influence specific cell fates in several developmental processes; however, the effect of oxygen levels on cell differentiation is thought to be context-dependent (14). Our data on CD133 expression in response to hypoxia were different from the previous study shown in glioma (5). The discrepancy might be explained by (*a*) a different cellular context in glioma from the others, because CD133 expressions of all cell lines including the WiDr, IM95, SNU16, OCUM1, 44As3, and DLD-1 cells were reproducibly down-regulated by hypoxic condition (Supplemental Fig. S1; Fig. 3*B*), whereas the U251 cells failed to exhibit the down-regulation, and by (*b*) the different detection methods in our study (Western blot and quantitative real-time RT-PCR) from the previous report (flow cytometry for CD133-positive cells).

The detailed mechanism responsible for the repressive role of HIF-1α on CD133 expression is not fully understood; one possible explanation is raised by MYC, which is also known as c-Myc. HIF-1α binds to MAX and renders MYC inactive, and HIF-1 (homodimers of HIF-1α and HIF-1β) activates the expression of MXI1 (MAX interactor 1), which binds to MAX and thereby antagonizes MYC function (11). Recent reports have shown that HIF-1α inhibits MYC activity, which is thought to have implications for stem cell function (15, 16). Whether MYC directly activates CD133 transcription remains unclear; our preliminary data indicate that a MYC-inhibitor suppressed CD133 expression in WiDr cells.[4] Because the gene amplification of MYC and MYCN is frequently observed in many cancers, the relations among MYC, HIF-1α, HIF-1β, HIF-2, and CD133 should be investigated in future studies.

In conclusion, we showed that the inhibition of mTOR signaling up-regulated CD133 expression, whereas HIF-1α induction under hypoxic conditions or DFO exposure down-regulated CD133 expression in gastrointestinal cancer cells. Our findings show a novel regulatory mechanism for the expression of CD133 involving mTOR signaling and HIF-1α, and these findings may contribute to our understanding of the stemness character of cancer stem cells.

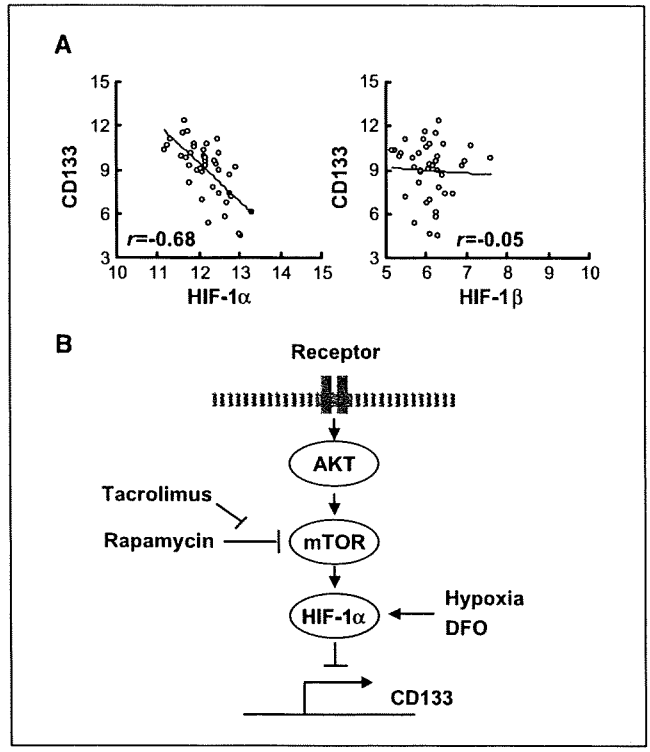

Figure 4. Inverse correlation between CD133 and HIF-1α in clinical samples of gastric cancer. *A*, the correlation between the expressions of CD133 and HIF-1α were analyzed in 40 clinical gastric cancer specimens using previously published microarray data. CD133 and HIF-1α were inversely correlated in gastric cancer ($r = -0.68$), whereas CD133 and HIF-1β were not ($r = -0.05$). *B*, proposed model depicting the involvement of mTOR signaling, HIF-1α, and CD133 expression. HIF-1α, a downstream molecule of mTOR, down-regulates CD133 expression at the transcriptional level in cancer cells.

Disclosure of Potential Conflicts of Interest

No potential conflicts of interest were disclosed.

Acknowledgments

Received 4/7/09; revised 6/2/09; accepted 6/30/09; published OnlineFirst 9/8/09.

Grant support: 3rd Term Comprehensive 10-Year Strategy for Cancer Control, the program for the promotion of Fundamental Studies in Health Sciences of the National Institute of Biomedical Innovation, and a Grant-in-aid for Scientific Research from the Ministry of Education, Culture, Sports, Science and Technology of Japan (19790240 and 19209018).

The costs of publication of this article were defrayed in part by the payment of page charges. This article must therefore be hereby marked *advertisement* in accordance with 18 U.S.C. Section 1734 solely to indicate this fact.

[4] Unpublished data.

References

1. Neuzil J, Stantic M, Zobalova R, et al. Tumour-initiating cells vs. cancer "stem" cells and CD133: what's in the name? Biochem Biophys Res Commun 2007;355:855–9.
2. Fan X, Matsui W, Khaki L, et al. Notch pathway inhibition depletes stem-like cells and blocks engraftment in embryonal brain tumors. Cancer Res 2006;66:7445–52.
3. Clement V, Sanchez P, de Tribolet N, Radovanovic I, Ruiz i Altaba A. HEDGEHOG-GLI1 signaling regulates human glioma growth, cancer stem cell self-renewal, and tumorigenicity. Curr Biol 2007;17:165–72.
4. Piccirillo SG, Reynolds BA, Zanetti N, et al. Bone morphogenetic proteins inhibit the tumorigenic potential of human brain tumour-initiating cells. Nature 2006;444:761–5.

5. Platet N, Liu SY, Atifi ME, et al. Influence of oxygen tension on CD133 phenotype in human glioma cell cultures. Cancer Lett 2007;258:286–90.
6. Chen HL, Pistollato F, Hoeppner DJ, Ni HT, McKay RD, Panchision DM. Oxygen tension regulates survival and fate of mouse central nervous system precursors at multiple levels. Stem Cells 2007;25:2291–301.
7. Hudson CC, Liu M, Chiang GG, et al. Regulation of hypoxia-inducible factor 1α expression and function by the mammalian target of rapamycin. Mol Cell Biol 2002; 22:7004–14.
8. Chiang GG, Abraham RT. Targeting the mTOR signaling network in cancer. Trends Mol Med 2007;13: 433–42.
9. Yamada Y, Arao T, Gotoda T, et al. Identification of prognostic biomarkers in gastric cancer using endoscopic biopsy samples. Cancer Sci 2008;99: 2193–9.
10. Takeda M, Arao T, Yokote H, et al. AZD2171 shows potent antitumor activity against gastric cancer over-expressing FGFR2/KGFR. Clin Cancer Res 2007;13: 3051–7.
11. Dang CV, Kim JW, Gao P, Yustein J. The interplay between MYC and HIF in cancer. Nat Rev Cancer 2008;8: 51–6.
12. Wouters BG, Koritzinsky M. Hypoxia signalling through mTOR and the unfolded protein response in cancer. Nat Rev Cancer 2008;8:851–64.
13. Danet GH, Pan Y, Luongo JL, Bonnet DA, Simon MC. Expansion of human SCID-repopulating cells under hypoxic conditions. J Clin Invest 2003;112:126–35.
14. Simon MC, Keith B. The role of oxygen availability in embryonic development and stem cell function. Nat Rev Mol Cell Biol 2008;9:285–96.
15. Koshiji M, Kageyama Y, Pete EA, Horikawa I, Barrett JC, Huang LE. HIF-1α induces cell cycle arrest by functionally counteracting Myc. EMBO J 2004;23: 1949–56.
16. Zhang H, Gao P, Fukuda R, et al. HIF-1 inhibits mitochondrial biogenesis and cellular respiration in VHL-deficient renal cell carcinoma by repression of C-MYC activity. Cancer Cell 2007;11:407–20.

Int. J. Radiation Oncology Biol. Phys., Vol. 76, No. 1, pp. 277–286, 2010

0360-3016/10/$–see front matter

ELSEVIER

doi:10.1016/j.ijrobp.2009.05.065

PHYSICS CONTRIBUTION

THE DEVELOPMENT AND CLINICAL USE OF A BEAM ON-LINE PET SYSTEM MOUNTED ON A ROTATING GANTRY PORT IN PROTON THERAPY

TEIJI NISHIO, PH.D.,*† AYA MIYATAKE, M.SC.,‡ TAKASHI OGINO, M.D.,* KEIICHI NAKAGAWA, M.D.,† NAGAHIRO SAIJO, M.D.,§ AND HIROYASU ESUMI, M.D.||

From the *Particle Therapy Division, Research Center for Innovative Oncology, National Cancer Center, Kashiwa; †Department of Radiology, Graduate School of Medicine, University of Tokyo; ‡Department of Nuclear Engineering and Management, Graduate School of Engineering, University of Tokyo; §Deputy Director, National Cancer Center, Kashiwa; and ||Director, National Cancer Center, Kashiwa

Purpose: To verify the usefulness of our developed beam ON-LINE positron emission tomography (PET) system mounted on a rotating gantry port (BOLPs-RGp) for dose–volume delivery-guided proton therapy (DGPT).
Methods and Materials: In the proton treatment room at our facility, a BOLPs-RGp was constructed so that a planar PET apparatus could be mounted with its field of view covering the iso-center of the beam irradiation system. Activity measurements were performed in 48 patients with tumors of the head and neck, liver, lungs, prostate, and brain. The position and intensity of the activity were measured using the BOLPs-RGp during the 200 s immediately after the proton irradiation.
Results: The daily measured activity images acquired by the BOLPs-RGp showed the proton irradiation volume in each patient. Changes in the proton-irradiated volume were indicated by differences between a reference activity image (taken at the first treatment) and the daily activity-images. In the case of head-and-neck treatment, the activity distribution changed in the areas where partial tumor reduction was observed. In the case of liver treatment, it was observed that the washout effect in necrotic tumor cells was slower than in non-necrotic tumor cells.
Conclusions: The BOLPs-RGp was developed for the DGPT. The accuracy of proton treatment was evaluated by measuring changes of daily measured activity. Information about the positron-emitting nuclei generated during proton irradiation can be used as a basis for ensuring the high accuracy of irradiation in proton treatment. © 2010 Elsevier Inc.

Dose–volume delivery guided proton therapy (DGPT), Beam ON-LINE PET system on rotating gantry port (BOLPs-RGp), Target nuclear fragment reaction.

INTRODUCTION

Proton therapy is a form of radiotherapy that enables the concentration of a dose onto a tumor by the use of a scanned or modulated Bragg peak. Therefore, it is very important to evaluate the proton-irradiated volume accurately.

Recently, to ensure the high accuracy of proton therapy, imaging studies of positron-emitting nuclei that are generated by target nuclear fragment reactions involving incident protons and nuclei from a patient's body have been performed (1–14). The annihilation gamma rays from the positron-emitting nuclei were measured by a positron emission tomography (PET) system (specifically a beam OFF-LINE PET system using commercial PET apparatus or PET-computed tomography [CT] apparatus postirradiation or a beam ON-LINE PET system in a proton treatment room). The beam OFF-LINE PET system using the commercial PET-CT apparatus has the advantage of being able to easily acquire fusion images and the ability to reconstruct three-dimensional images. However, the time required for the movement of the patient to the PET room (10–30 min) and the resulting deterioration of the statistical accuracy of the acquired data are large disadvantages. With the beam ON-LINE PET system, capturing a large view and the acquisition of three-dimensional images are difficult because of geometrical problems caused by the beam direction and the PET apparatus (7, 15, 16).

Reprint requests to: Teiji Nishio, Ph.D., Particle Therapy Division, Research Center for Innovative Oncology, National Cancer Center, Kashiwa 6-5-1 Kashiwano-ha, Kashiwa-shi, Chiba 277-8577, Japan. Tel: (+81) 4-7133-1111; Fax: (+81) 4-7134-7048; E-mail: tnishio@east.ncc.go.jp

Conflict of interest: none.

Supported by Health and Labour Science Research Grants from the Japanese Government.

Acknowledgment—The authors would like to thank the staff members of the Proton Radiotherapy Department of the National Cancer Center, Kashiwa for their help and the members of SHI Accelerator Service, Ltd., and Accelerator Engineering, Inc., for operating of the proton apparatus. We also acknowledge T. Okamoto of Hamamatsu Photonics, K. K., T. Tachikawa of Sumitomo Heavy Industries, Ltd., and H. Oka of SGI Japan, Ltd., for their technical support.

Received Jan 6, 2009, and in revised form May 28, 2009. Accepted for publication May 29, 2009.

The ability to take daily PET images with a high statistical accuracy while the patient remains in the proton irradiation room is a large advantage. Besides, availability of a cone beam (CB) CT system or CT apparatus in the irradiation room can offer the possibility of daily and in situ monitoring of the patient's anatomy. A prototype beam ON-LINE PET system (BOLPs) was previously constructed for basic research (10), and verification of the proton-irradiated volume in a patient's body was confirmed using a PET apparatus and a PET-CT apparatus (beam OFF-LINE PET system) (13).

A BOLPs mounted on a rotating gantry port (BOLPs-RGp) was constructed in our proton treatment room. Activity measurement and PET imaging were performed in 48 patients with tumors of the head and neck, liver, lungs, prostate, and brain during proton treatment at our facility. The position and intensity of the activity were measured daily using the BOLPs-RGp immediately after proton irradiation. Using the activity measurement, we were able to confirm whether the proton beam irradiation of the tumor was reproducibly performed during the treatment period. Moreover, changes in the activity distribution were observed as the volume of the tumor changed, and these changes were related to the delivery dose, changes in the body shape and position of the patient, and the physiologic changes. The PET images from the BOLPs-RGp were sufficient to provide high-quality proton treatment.

METHODS AND MATERIALS

Design of a beam ON-LINE PET system mounted on an RGp

Via the detection of pairs of annihilation gamma rays emitted from the generated radioactive nuclei of a patient's body, the BOLPs-RGp is designed to determine the position and activity of the positron-emitting nuclei generated in patients by proton irradiation. Figure 1 is a picture of the BOLPs-RGp. The BOLPs-RGp was developed as a standardized system for use with proton therapy devices. During proton therapy, the detector heads have many degrees of freedom and the system allows remote control adaptation to each new proton beam condition and a patient's position. As a result, the measurement of the activity distribution is simple.

A planar positron imaging system (Hamamatsu Photonics K. K., Hamamatsu, Japan) (17) was newly arranged for the BOLPs-RGp. In comparison to the system used previously (10), the 24 detector units mounted on each detector head were increased to 36 detector units, and each unit was composed of 11 × 10 arrays of BGO ($Bi_4Ge_3O_{12}$) crystals with a crystal size of 2 × 2 × 20 mm^3. Furthermore, the 2,400 crystals were increased to 3,600 crystals. The gap of each unit became 3.3 mm from 11.0 mm for minimizing dead space in the detector. The field of view (FOV) became 164.8 × 167.0 mm^2 from 120.8 × 186.8 mm^2. The maximum field size is 185.0 × 185.0 mm^2 in the rotating gantry port with the BOLPs-RGp. Therefore, the FOV can almost cover each treatment site of the head and neck, liver, lungs, prostate, and brain for a proton treatment in our facility. However, in case of prostate, the depth activity distribution is not measured in the entrance of the incident proton beam. The BOLPs-RGp was mounted on and the center of its detection area was aligned with the iso-center of the rotating gantry in the treatment room of the proton therapy facility at our center. A PET image reconstructed by a back-projection method

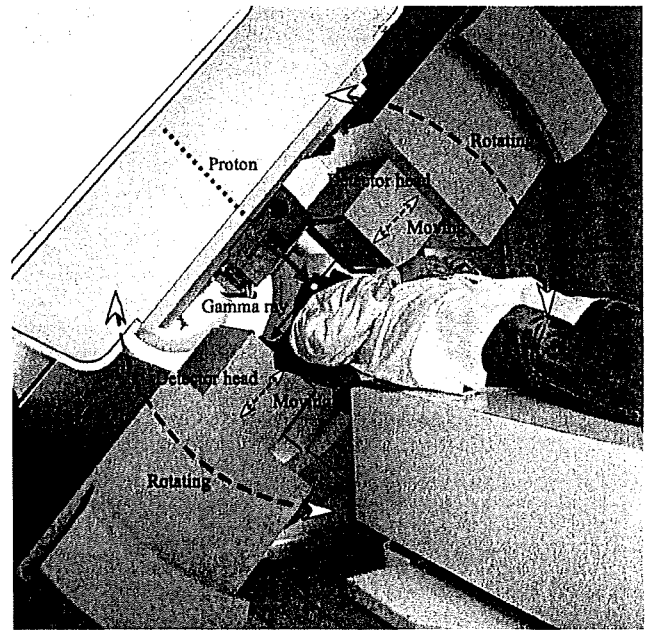

Fig. 1. Setup of the BOLPs-RGp, which is mounted on the rotating gantry port of our proton treatment room.

along the axis of the proton beam direction is always included in the FOV of the opposing detectors together with the axis of the rotating angle of the gantry system. The distance between the two opposing detector heads of the BOLPs-RGp can be adjusted from 30 to 100 cm. When the activity is not being measured, the detector head is stored inside the wall of the gantry device. The position resolution of this system is about 2 mm for the full width at half maximum in the case of use of ^{22}Na point source. The maximum data collection rate for the coincident detection of pair annihilation gamma rays is about 4,000 counts/s/cm^2 (kcps/cm^2). The accuracy of the measurements of activity distribution by this system was verified by a prototype beam ON-LINE PET system (10). The measured data are stored using in the software's list mode format. The activity image is renewed every second. The information of the on-off time points of beam irradiation is recorded in the data, and the image can be restructured according to this information. The PET data from the irradiation field of each patient are managed throughout each treatment day.

The detection efficiency of the distance between the detector heads was calibrated by using the thin-flat acrylic container filled with ^{18}F-solution. The calibration is used for a correction of the imaging uniformity and the detection sensitivity. The attenuation coefficient of 511-keV gamma rays in the patient's body was calculated by the patient's CT image data. They are used for a construction of the activity imaging. The correction of the photon scattering in the patient's body is not considered for the activity imaging. Furthermore, the photons scattered in the patient's body outside the FOV are detected by the effect of the geometry of the detector head. Therefore, the activity image is contaminated by about 10% background in this system. As the result, the position resolution of the activity distribution will become large more than 2 mm in the clinical case of a proton therapy.

Activity measurement in a patient during proton treatment

The measurement of activity was performed daily in 48 cases involving tumors of the head and neck, liver, lungs, prostate, and brain

using the BOLPs-RGp. The position and intensity of activity were measured during the 200 s immediately after proton irradiation using the trigger signal of the beam-off time. The measurement was performed using the shortest possible distance between the two opposing detector heads of the BOLPs-RGp for each patient. The average distance of the detector heads was 40 cm for the head and neck and the brain, 70 cm for the liver and the lungs, and 50 cm for the prostate. The time of 200 s after proton beam irradiation was chosen according to the intensity of activity estimated from the results of other studies (10, 13). The activity data obtained during proton irradiation were not used for PET imaging. Various types of background radiation (X-rays, gamma rays, and neutrons) occur during proton beam irradiation, and the quality of the activity image becomes markedly worse in their presence (2, 10, 15, 16). Furthermore, high radiation decreases the accuracy of the detector.

Verification of activity measurement was performed in 18, 4, 15, 10, and 1 cases involving tumors of the head and neck, the liver, the lungs, the prostate, and the brain, respectively. The typical fractional dose is 2.5 Gy equivalents (GyE = Gy × the relative biologic effectiveness: [= 1.1 = constant]) for the head and neck, 3.8 GyE for the liver, 4.0 GyE for the lungs, 2.0 GyE for the prostate, and 2.5 GyE for the brain in our facility. The irradiated field is typically planned with three fields in the head and neck and two fields in other sites. Furthermore, the typical number of irradiated field per fractional dose is one in the head and neck, liver, and prostate, and two in the lungs. The fractional dose was delivered over an irradiation time of 10–300 s. The proton beam irradiation was synchronized with the organ motion caused by respiration in the liver and the lungs.

Procedure for clinical use of activity image

A flow chart of procedure for clinical use of the BOLPs-RGp is shown in Fig. 2. In the clinical use, the main operation is to take an activity image every day and compare the activity image of the first day of treatment with each activity image during the comparatively long period of the treatment. If the difference of both the images is confirmed by reducing of the tumor size and changing of the body shape, then the new dose distribution is obtained from redose calculation of the plan on a new CT image acquisition, and the first proton treatment plan is immediately corrected to the new plan. As a result, proton treatments of high accuracy can be offered to the patient by keeping of the planned dose delivery.

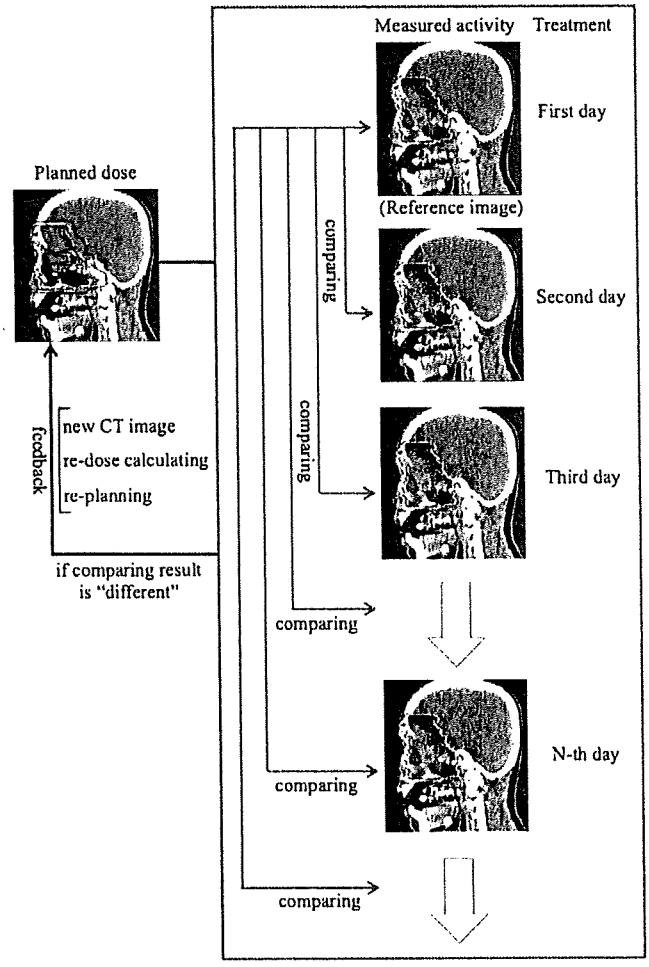

Fig. 2. Flow diagram of the procedure for the clinical use of the BOLPs-RGp.

RESULTS

Estimation of the measurement time for PET imaging

An estimation of an appropriate measurement time for PET imaging was performed using the measured activity data from tumors of the head and neck. The proton beam conditions were as follows: an energy of 120 MeV, a spread out of Bragg peak (SOBP) of 80-mm width, a gantry angle of 340°, a fractional dose of 2.5 GyE, and an irradiation time of 24 s. The distance between the detector heads was 70 cm, and the detection rate of the activity was 1.5 kcps. The left panel of Fig. 3 shows the number of detection events per volume during the detection period after proton beam irradiation. The statistical error (= standard deviation/mean value) decreased as the detection time increased. The error was 2.8% for a 200-s detection time, 3.0% for 150 s, 3.4% for 100 s, and 4.4% for 50 s. The right panel of Fig. 3 shows PET images taken using detection times of (a) 0, (b) 50, (c) 100, and (d) 200 s.

PET images of each treatment site

Typical PET images obtained by the BOLPs-RGp are shown for each case involving tumors of the head and neck, the liver, the lungs, the prostate, and the brain. Figure 4 shows the calculated dose distribution and the measured activity distribution on the first treatment day. The beam irradiation parameters were shown in Table 1. The PET images were obtained during the 200 s after proton beam irradiation. The mean detection rates of the activity generated in the proton beam irradiated volume were 1.58, 1.39, 0.53, 1.08, and 1.85 kcps, respectively. The color line and wash normalized to the iso-center show the dose distribution and activity distribution, respectively. By comparing and verifying between the calculated dose distribution and the measured activity distribution, it can be confirmed visually and roughly that the proton beam has irradiated the tumor. In cases of the liver and the lungs, the length of beam irradiation time is adjusted according to the stability of respiration on the treatment day and the patient. By the effect of organ motion, the number of